Master's Thesis

Synthesis of Aminophosphine-based InP Nanocrystals and InP@ZnS Quantum Dots Through Versatile Steel Microfluidic Reactor System

Dongwoo Seo

Department of Chemical Engineering

Graduate School of UNIST

2018

Synthesis of Aminophosphine-based InP Nanocrystals and InP@ZnS Quantum Dots Through Versatile Steel Microfluidic Reactor System

Dongwoo Seo

Department of Chemical Engineering

Graduate School of UNIST

Synthesis of Aminophosphine-based InP Nanocrystals and InP@ZnS Quantum Dots Through Versatile Steel Microfluidic Reactor System

A thesis/dissertation
submitted to the Graduate School of UNIST
in partial fulfillment of the
requirements for the degree of
Master of Science

Dongwoo Seo

12/07/2017

Approved by

Advisor
Jongnam Park

Synthesis of Aminophosphine-based InP Nanocrystals and InP@ZnS Quantum Dots Through Versatile Steel Microfluidic Reactor System

Dongwoo Seo

This certifies that the thesis/dissertation of Dongwoo Seo is approved.

12/07/2017

Signature

Advisor: Jongnam Park

Signature

Kwangjin An: Thesis Committee Member #1

Signature

Jiseok Lee: Thesis Committee Member #2

Abstract

Quantum dots (QDs) are applied in various fields including light-emitting devices, bio-sensing due to their unique optical properties. Although cadmium-based quantum dots have high photoluminescence quantum yield and narrow emission line widths, use of cadmium in synthesis process could bring related environmental issues and restrict quantum dot application to certain fields like in vivo bio imaging. To solve those issues, III-V quantum dots like indium phosphide quantum dots (InP QDs) are considered as substitution for cadmium-based QDs. However, most of recent studies of InP QDs used tris(trimethylsilyl)phosphine ($(TMS)_3P$) as phosphine precursor, which is expensive, highly toxic and creates pyrophoric substance in contact with air.

For general QD synthesis, lab-scale batch processes using typical flasks are mostly conducted. However, due to difficulty in scale-up and time-consuming preparations, those processes are inappropriate for continuous mass production.

In III-V QD synthesis, especially for InP QDs, phosphine precursors like aminophosphines are considered as replacement for $(TMS)_3P$ with relatively lower price and higher stability in the air. Also, due to the advantages such as efficient controls of temperature and high surface-to-volume ratio, microfluidic reactors are starting to gain attention as suitable media for various nanoparticle synthesis.

For these reasons, this article studies about the synthesis of InP nanocrystals (NCs) and QDs using aminophosphine as phosphine precursor and steel-based microreactor system. Application of microreactor in the process showed the possibility of continuous synthesis of InP NCs and QDs, as well as simple tuning of 1^{st} exciton peak of the products via changing the variables such as flow rate, temperature, halide exchange of indium precursor and dodecanethiol (DDT) addition. Synthesis of InP@ZnS Core@Shell-structured QDs is also conducted in microreactor, showing similar PLQY of the product compared to that of the QDs produced from batch reactor.

Blank Page

Contents

List of figures

Chapter I : Introduction of microfluidic reactor and its application on nanocrystal synthesis

1.1. Definition of microfluidic reactor

'Microfluidic reactor' (MFR) means the reactor which its volume is very small, in the general range of microliters to nanoliters. Nowadays, MFRs are applied in various fields including physics, chemistry and biology. MFRs show unique behaviors different from conventional batch reactor and continuous reactor.

The unique behavior of MFRs is based on their small volume and channel size. Small volume and channel size of reactors make properties like surface tension, energy dissipation, resistance between channel and fluid dominant in the system. Study of microfluidic reactor includes the design of reactor structures, as well as the study of unique behaviors and characteristics of the reactors.[1-3]

Channel diameter of microfluidic reactors typically have the size of 100 nm to 500 um. Due to its small size of channel and volume, fluids in the reactor process with behavior of laminar flow with low Reynold number. In the matter of mixing in multi-flow reaction using laminar flow, diffusion between fluid flows became dominant.[4] However, mixing mainly occurred by diffusion takes long time, which is inefficient. To overcome the problem of mixing in the microfluidic reactors, segmented flow made from immiscible liquids or gas and liquid phase flow is applied to increase the mixing efficiency on the each of segmented slugs. Also, droplet flow is applied to the system to enhance the efficiency of mixing, which is similar from segmented flow.[5,6]

Advantages of MFR is based on its small volume. First, with small volume, temperature and heat on the reactors can be easily controlled since heat transfer and other transport phenomena in the reactors are occurred much faster and more efficient than that of conventional reactors. Also, microfluidic reactors require small amounts of reagent to proceed reactions. That means, it can save the energy and reagents from each reaction and can handle toxic and reactive substances much safer, especially when the situations like reactor leakage happens.[7,8] Lastly, microfluidic reactors are suitable for applying pressurization process.[9]

Clogging of channels and inhomogeneity of surface-to-volume ratio due to damaging and corrosion are considered as disadvantages,[10,11] but those problems can be solved from changing the structural

design and flow behaviors of the reactors.[12,13]

In the matter of producibility, microfluidic reactor's small volume can be a disadvantage because of its low throughput. However, through increasing flow rate by changing reactor substances and parallelization of multiple reactors, which called Scaling-out, throughput of microfluidic reactors can be increased. Many studies already published about those solutions for enhancing the producibility of the reactors.[12,14]

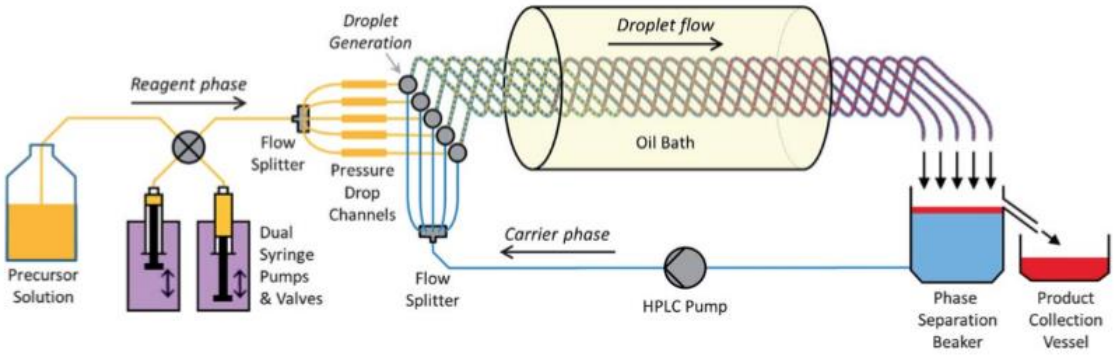

Figure 1. Schematic of multi-microchannel droplet reactor[12]

1.2. History of microfluidic reactor

The origin of the microfluidic reactor goes up to late 1960s, which based on the gas chromatography used at Stanford university and inkjet printer invented by IBM.[15]

However, the concept and research of microfluidic reactor was started much earlier, which is the study of Jean Leonard Marie Poiseuille and Gotthilf Heinrich Ludwig Hagen about fluids in capillary and the well-known Hagen-Poiseuille equation based on that study.

After the prototypes of microfluidic reactor and related devices were reported in late 1960s, 3D printing invented in 1980s showed a possibility about crafting the microfluidic reactor that can be used in various chemical reactions. 3D printing enabled the fabrication of the reactors with third-dimensional structure and integrated multilayer reactors in simple way. Later, 3D printing also helped to set the standardization of microfluidic reactors.[16]

The first integrated micro-volume component devices based on silicon wafer was created using silicon etching process for mainly creating microelectronic devices This new devices called ‘MEMS’ (Micro Electro Mechanical Systems), showed potential possibility of applying on the many industrial fields.

In 1990s, MEMS were widely applied on fields such as biology, chemistry and pharmacology. Also, microfluidic reactors related to Lab-on-a chip were starting to be created. Since controlling and analyzing the certain flow patterns in the microfluidic reactors are important to MEMS, those applications in various field of study triggered the revolution of the research on microfluidic reactors.[17] After that, the fundamental study about the fabrication of miniaturized capillary for chemical analysis based on electrophoresis by Andreas Manz and the prototype of polydimethylsiloxane (PDMS) -based microfluidic reactor system created by George Whitesides and coworkers were published. Simple and fast fabrication and design of microfluidic reactor using photolithography introduced at the study of George Whitesides had a huge impact on the fabrication methods and related studies.[18]

Nowadays, many types of microfluidic reactors fabricated from 3D printing and other methods are broadly used in various fields, especially in the field of biology and chemical synthesis. Lately, with the advantage of versatility on fabricating microfluidic reactors, the reactors also applied in fine chemistry and unique pharmacology.

1.3. Fabrication of microfluidic reactor

Microfluidic reactors can be fabricated from various materials. Characteristics of the reactor can be different from its material used in fabrication.

Steel-based microfluidic reactors have the advantage that they can operate in the extreme conditions, such as high-temperature and high-pressure condition. Also, with materials like steel capillary, it can design the reactor system in simple and convenient way. However, steel-based reactors can be corroded by certain chemicals like strong acid. Metals resistant to acids and chemicals are required to fabricate such reactors operating with those substances.[19,20]

To endure such chemicals, microfluidic reactors can be fabricated by using silicon, glass or ceramics.[21,22] These types of reactors can also be used in high-temperature condition. Also, those materials are chemically stable, which have high resistance to acid and such chemicals. Especially for Silicon-based microfluidic reactors, high thermal conductivity of silicon makes the heating and controlling the temperature on the reaction system more efficient. Also, when combined with glass, silicon-based microfluidic reactors can achieve visibility while maintain advantages mentioned above. Typically, those silicon-glass hybrid reactors are fabricated with method inducing chemical bonding between the materials such as anionic bonding, leading to sustain at the high temperature and pressure conditions. However, fabrication of those systems is complex and expensive. Reactor failure when using strong base can also be the problem. Glass microfluidic reactors have low thermal conductivity due to its fabricating material, which could be not suitable for reactions required efficient heating.[21,23]

Besides the steels and ceramics as the fabrication materials, polymer can be the material for crafting the reactors. Poly(dimethylsiloxane) (PDMS) is mainly used to fabricate the microfluidic reactors, especially for biology application. Polymer-based microfluidic reactors have advantages of easy and simple fabrication owing to method like 3D printing, showing the possibility of mass production of the reactors. However, swelling and dissolution of reactor when using organic solvent restrict its application.[24] Using fluoropolymer as reactor material can be the solution, but in that case, weak binding force between each polymers and polymer-glass makes the reactor unusable at the pressurized reactions.[25]

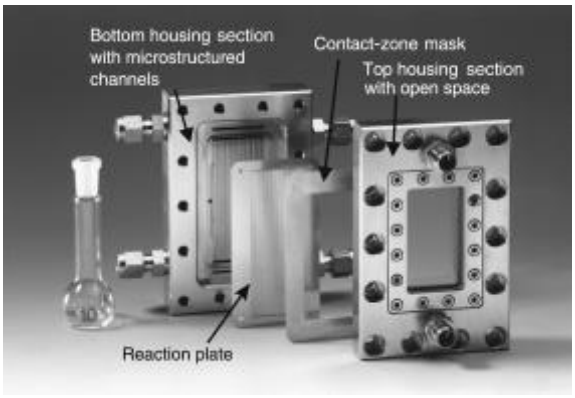

Figure 2. Photograph of steel-based multichannel droplet reactor[20]

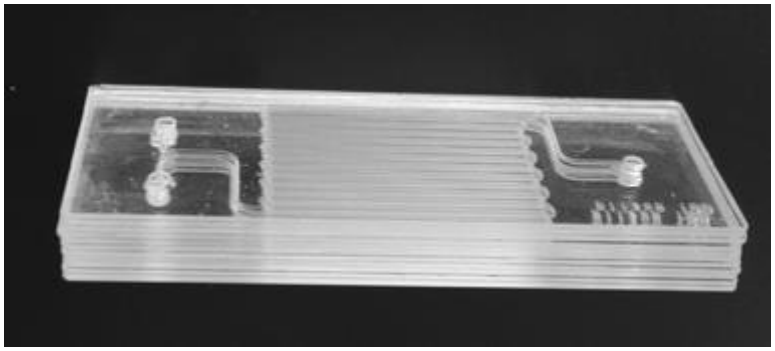

Figure 3. A photograph of the ten-layer, pile-up glass microreactor[22]

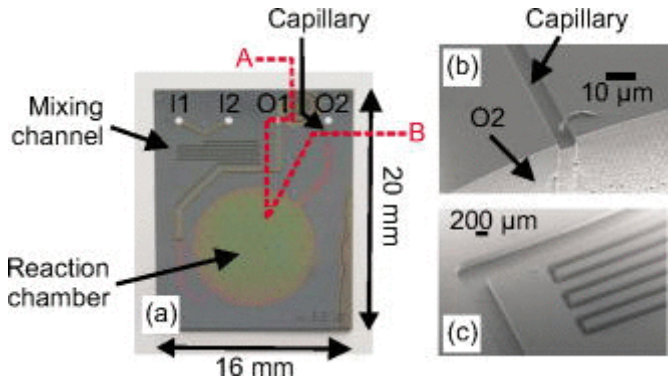

Figure 4. a) Photograph of silicon-based reactor with inlets and outlets b) Scanning electron micrograph of the junction between the capillary and the outlet c) Scanning electron micrograph of the mixing channel[26]

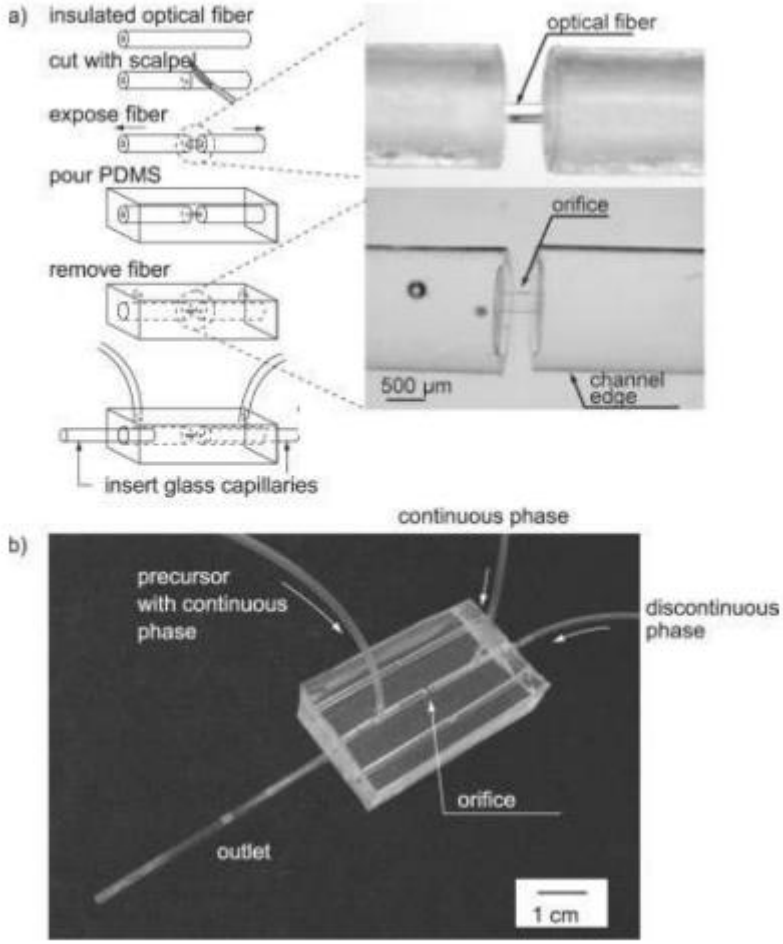

Figure 5. a) A scheme depicting the fabrication process of the AFFD. b) An image of the final AFFD[27]

1.4. Application of microfluidic reactor on nanocrystal synthesis

Applications of the microfluidic reactors are previously mentioned. Among the applications, there are numerous studies about synthesis of nanoparticles using the microfluidic reactors.

Optical nanoparticle synthesized applying microfluidic reactors are mainly II-VI quantum dots (QDs) like cadmium-based QDs. With the chip microreactor and capillary, Yang at el. designed the continuous system of synthesizing CdSe@ZnS Core@Shell-structured quantum dot. Also, Kwon at el. crafted the continuous microfluidic reactors made from single capillary for ZnSe nanocrystals (NCs) synthesis.[28-30] Also, for the synthesis of cadmium-based NCs and QDs, there are many studies about microfluidic reactors applying liquid-gas segmented flow and droplet flow to change the flow patterns, enhancing the quality of the products by removing inhomogeneity between nanoparticles in the middle of reaction.[31-33]

Studies about synthesizing III-V nanocrystals such as Indium phosphide (InP) on the microfluidic reactors are also conducted. By using silicon-Pyrex hybrid microreactor, Baek at el. succeeded the synthesis of InP NCs at the high temperature, high pressure conditions, while changing the reaction temperature and the flow rate and flow composition of reagent flow.[9] Similar from synthesis of cadmium-based NCs, micro systems made of single capillary or semi-batch process are also used to synthesize the InP NCs.[34,35]

Besides, Capillary microreactor system for synthesizing the $CsPbX_3$ perovskite NCs and QDs, microfluidic systems for VI-IV quantum dots and the system for graphene quantum using microfluidizer are also created, proving that there are numerous on-going studies conducted for nanoparticle synthesis using microfluidic reactors and related devices and systems.[36-38]

For extension of the nanoparticle synthesis on microfluidic reactors, purification processes of crude nanoparticle solution using microchannels and related systems are proposed by Lim at el., applying microchannel system with electrophoresis to continuously process the crude solution, while Shen at el. designed the microchannel system based on liquid-liquid extraction and membranes. These researches showed that the potential of the microfluidic reactor systems for integrating the entire chemical synthesis process on the one continuous system, while saving time and resources used in typical batch-based purification processes such as centrifugation.[39,40]

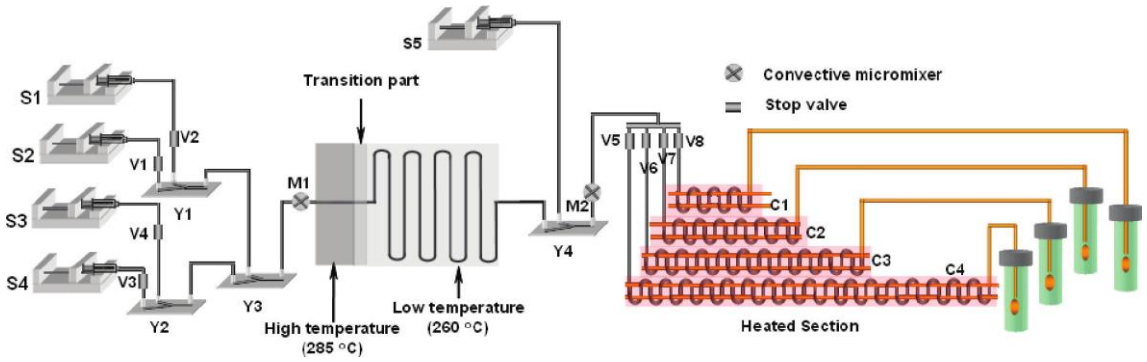

Figure 6. Schematic of the microfluidic reaction system for the continuous synthesis of CdSe/ZnS and CdS/ZnS NCs[28]

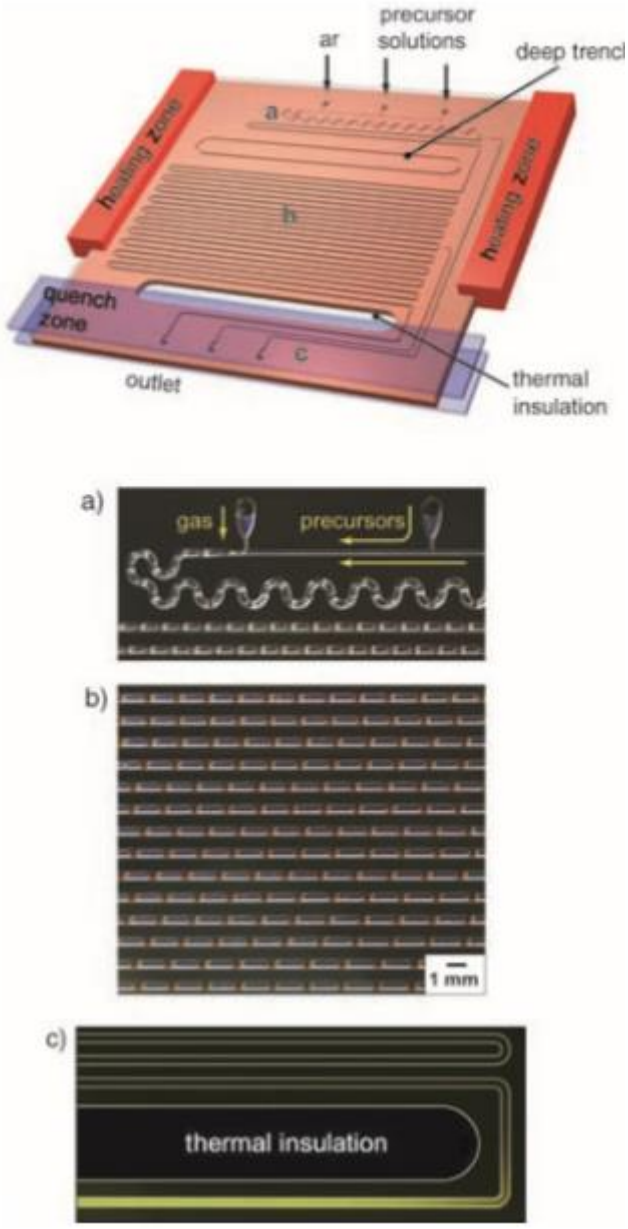

Figure 7. Reactor with heated reaction region and cooled outlet zone, a through-etch section ensures that the two regions are thermally isolated; a) heated inlets b) main channel section c) time-exposure image of the cooled outlet region under UV irradiation[31]

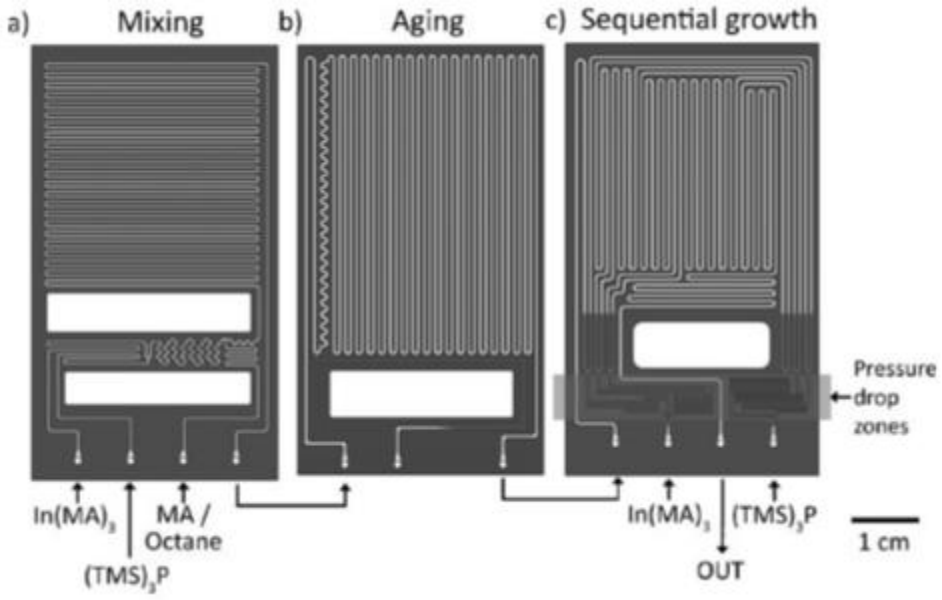

Figure 8. Three-stage high-temperature and high-pressure microfluidic system for synthesis of InP NCs a) mixing stage, b) aging stage c) sequential injection stage[9]

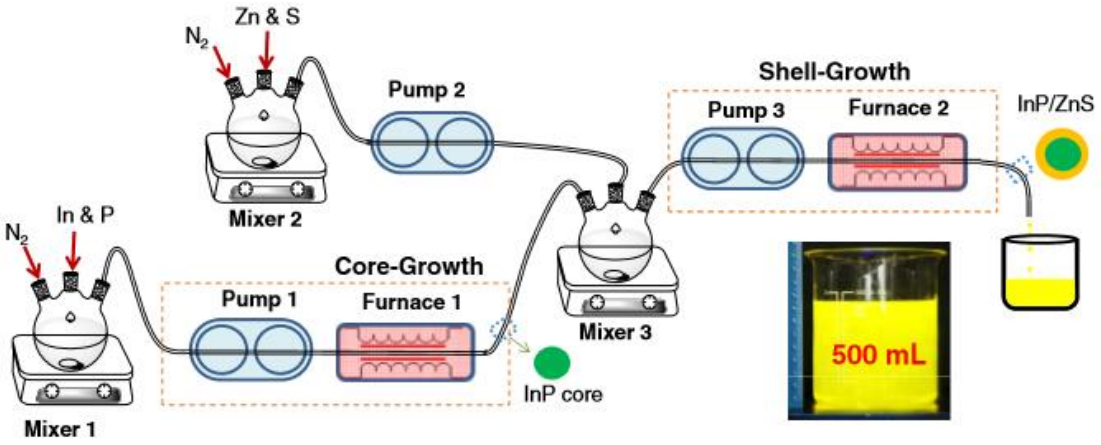

Figure 9. Schematic of a hybrid-flow reactor for synthesis of InP@ZnS QDs[35]

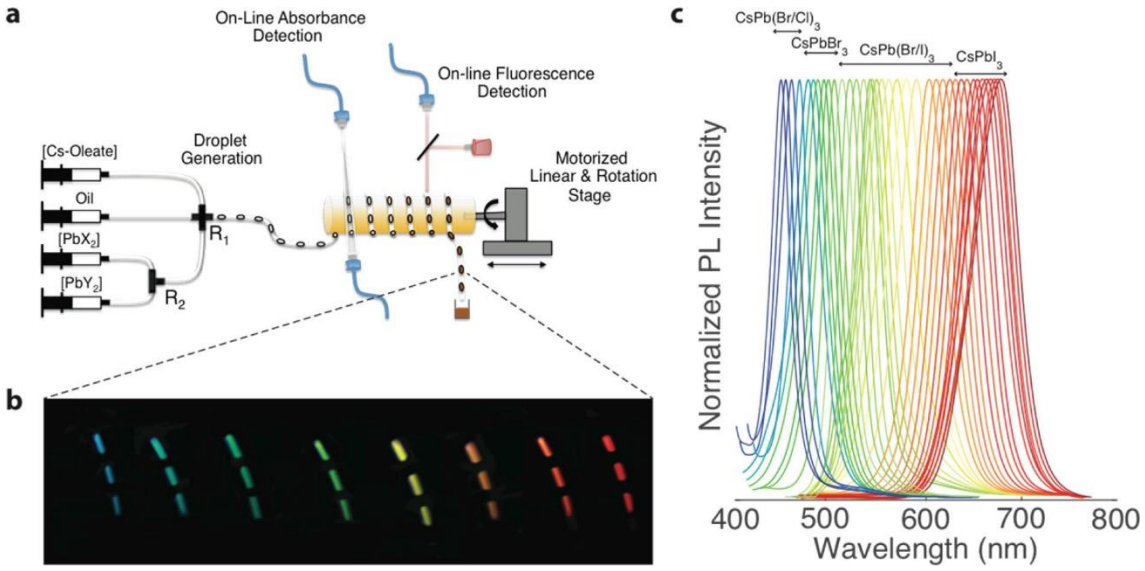

Figure 10. a) Illustration of the droplet-based microfluidic platform for synthesis of $CsPbX_3$ perovskite NCs b) Image of the generated droplets after exiting the heating zone taken under UV excitation c) Online fluorescence spectra of CsPbX3 NCs[36]

Chapter II : Synthesis of InP nanocrystals via microfluidic reactor

2.1. Introduction

Quantum dots (QDs) are widely used at semiconductors, optical devices[41-43], Bio-imaging technologies[44-46] and solar cells[47,48].

Among the various QDs synthesized until today, many studies and researches mainly focused on cadmium-based QDs such as cadmium selenide QDs (CdSe QDs) and cadmium sulfide QDs (CdS QDs) as the subjects for QD synthesis, because cadmium-based QDs have high photoluminescence efficiency and selectivity, while having broad emission ranges.[49,50]

Besides those II-VI quantum dots, III-V quantum dots like indium phosphide QDs (InP QDs) and organic, inorganic or organic/inorganic hybrid perovskite NCs with simple synthesis methods and high photoluminescence efficiency, narrow FWHM and broad emission ranges are also considered as new materials for optical devices.[51]

Although cadmium-based QDs have many advantages such as narrow FWHM and simple band-gap control, use of cadmium in synthesis may induce the environmental issues, restricting the ranges of application. This is mainly due to international regulation about environmental issues and concerns about safety of cadmium-based QDs as tools for bio-imaging and crafting electronic devices.[52-54] $CsPbX_3$ perovskite QDs have similar problems because of lead in the products.[53,55] Also, unlike the cadmium-based QDs which show high stability in the air, perovskite NCs and QDs show low stability, which makes them hard to commercialize without additional treatments.[53,56-58]

To resolve those problems, InP QDs are considered as the substitution to QDs previously mentioned. Relatively broader FWHM and lower photoluminescence efficiency compared to that of cadmium-based QDs are pointed as problems, but thanks to many studies, the properties of InP QDs are getting enhanced through additional methods. From those, the results of InP QDs with high photoluminescence and narrow FWHM are being published. Unlike cadmium-based QDs and lead-based perovskite QDs, InP QDs are free from environmental issues related to heavy metals and can be used at in vivo applications.[52,59-61]

In typical InP NC synthesis, tris(trimethylsilyl)phosphine ($(TMS)_3P$) is mainly used as phosphine precursor. But the problem is, $(TMS)_3P$ is expensive and highly reactive, also pyrophoric in the air.[62]

In the matter of synthesis process, process which injects the phosphine precursor in the middle of reaction, called 'Hot-injection method', is mainly used in lab-scale or batch-scale reaction. However, in the larger scale system, the method could be inappropriate because of the issues about heat and mass transfer in the reaction system, which can lead to temperature and concentration gradient to synthesize inhomogeneous products. Synthesis techniques like 'heating-up method', which put all precursors at the first of process, are proposed,[63-65] but they cannot remove the problems induced by temperature and concentration gradients.

To solve the problems, phosphine precursors based on aminophosphine, like tris(dialkylamino)phosphine are used to replace typical $(TMS)_3P$. Aminophosphines are inexpensive and relatively stable under the atmosphere compared to $(TMS)_3P$.

Studies about InP QD synthesis using aminophosphine and corresponding mechanisms are already in progress, in fact, there are cases of synthesizing high-quality InP QDs with aminophosphine.[52,62,66] Also, from recent studies, aminophosphine-based InP QDs show the possibility of applying LaMer model, which explains about the mechanism of II-VI NC formation. Those results could solve the problem about broad size distribution of InP NCs caused by high reactivity of phosphine precursor if applied properly.[67]

For scale-up issues in conventional batch-based processes, continuous synthesis using microfluidic reactors can be the solution. There are already many studies published about use of microfluidic reactors on continuous synthesis of various QDs, in both small and large scale.[9,12,28,30,31,32,36,37,68] However, there is no results of applying aminophosphine-based InP NCs synthesis on continuous microfluidic reactors.

In this study, aminophosphine-based synthesis of InP NCs and InP@ZnS core@Shell-structured QDs using stainless steel microfluidic reactor is discussed. The study contains fast and continuous synthesis of those nanoparticle, with the characteristics and behaviors of the reactor and its products through changing factors.

2.2. Experimental session

2.2.1. Overall setup of microfluidic reactor system

Figure 11 shows the schematics of the reactor and its system. The shape of the channels is sinusoidal and each reactor parts are attached physically with bolts.

Reagents are injected into the system with Harvard Apparatus PHD 2000 HVP Programmable Syringe Pump 70-2023 and 20 ml Harvard Apparatus steel syringes. Syringes and reactor parts are connected by 1/16" SUS316 tubes. Volume of the reactor is about 160 μl, with channel length and height of 1 mm. The dimension of each reactor plates is 100 X 55 X 12 mm, as size of upper and lower plates are same. To prevent the leakage result from physical attachment of the plates with bolts, gasket made of multilayers of Teflon tapes is added. Temperature control of reactor system is conducted by feedback controller, which probe is added between the each of reactor plates with the gasket.

For this system, 1-Octadecene (ODE) is used to clean the channels. Figure 12 shows the comparison between ODE which passed through newly formed channels and ODE passed the fully-washed channels through absorption graphs. According to the graphs, there are no differences between the results. Therefore, it proves that the reactor can be recycled through cleaning with the pure ODE.

The shape of channels is sinusoidal. Sinusoidal shape is typically used in design of microreactor channels, since it can increase the surface-to-volume ratio of the reactor to enhance the heat transfer.

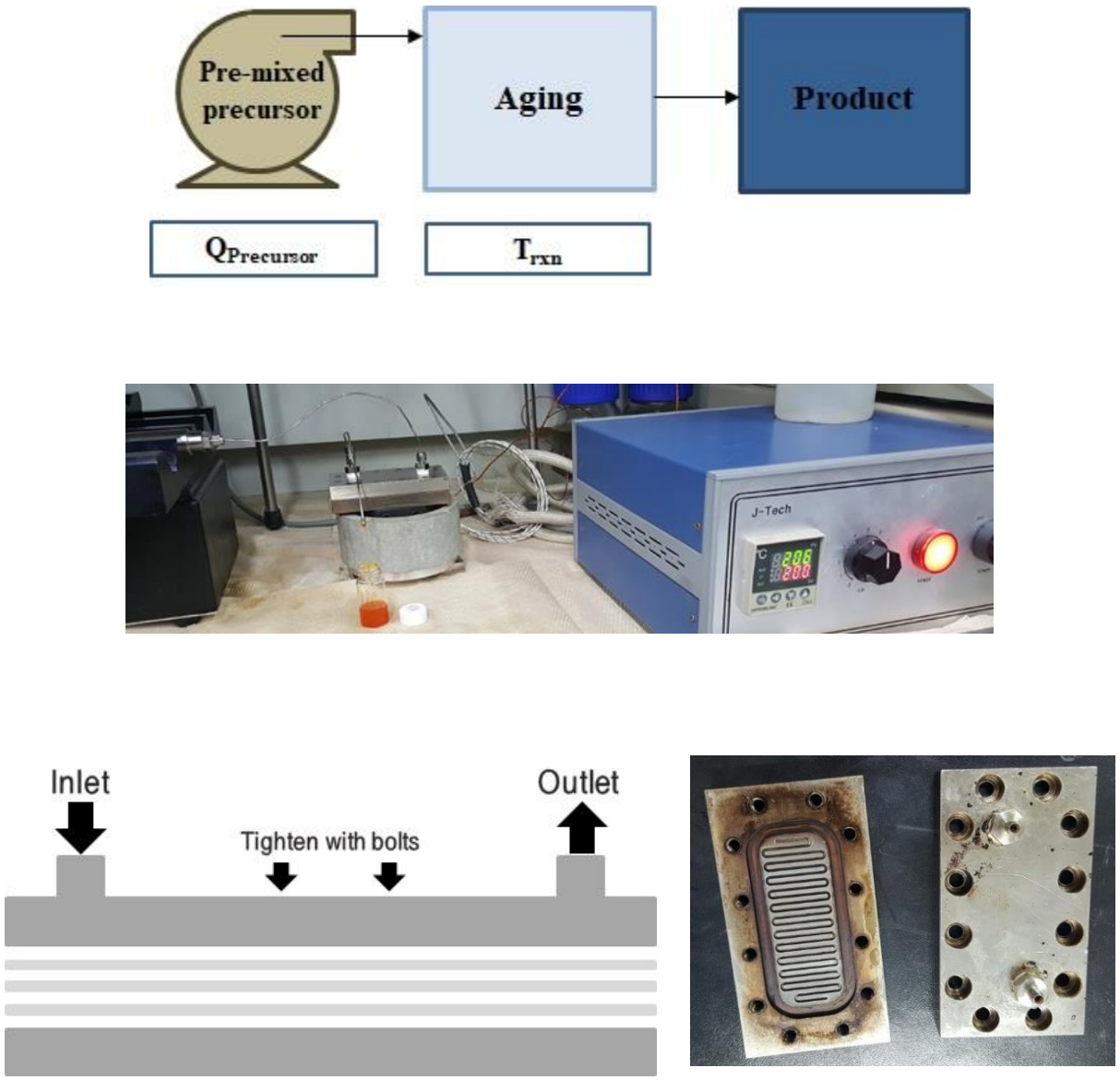

Figure 11. Schematics and images of InP NC synthesis microfluidic reactor system and structure of the reactor

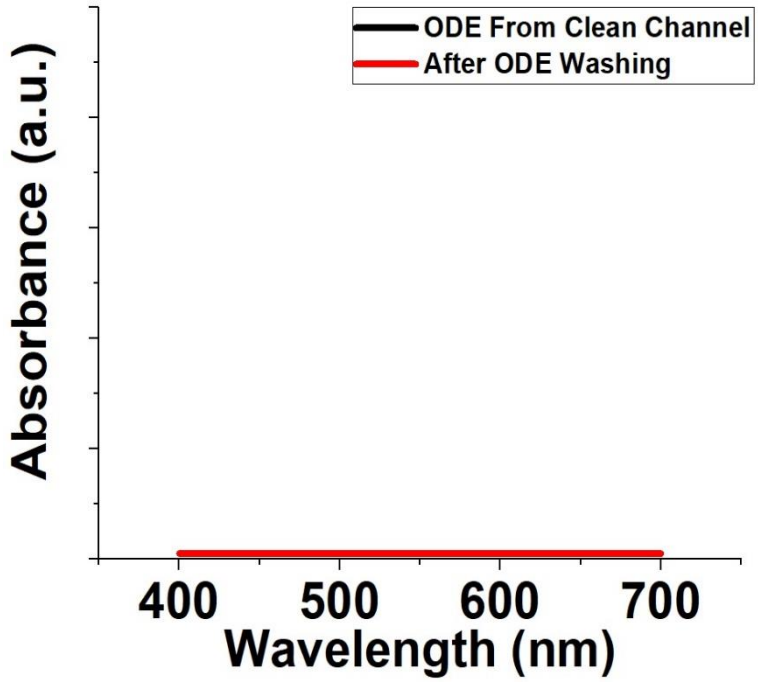

Figure 12. Absorption graph of ODE from clean channel and ODE after used in channel washing

2.2.2. Chemicals

Indium(III) chloride ($InCl_3$), Zinc chloride ($ZnCl_2$), Oleylamine (97%) (OAm), tris(diethylamino)phosphine (DEAP), tert-dodecanethiol and 1-Octadecene (ODE) are purchased from Sigma-Aldrich. Indium (III) bromide ($InBr_3$) and Indium (III) iodide (InI_3) are purchased from Strem. All the chemicals are used without further purification.

2.2.3. Preparation of stock solutions

$InCl_3$ 0.6 g, $ZnCl_2$ 1.8 g and 30 ml of oleylamine are prepared in 100 ml 2-neck round bottom flask under inert conditions. For degassing, prepared solution is heated to 120 ℃ for 90 minutes. After temperature of the mixture dropped down to RT, 2.76 ml of DEAP is injected under inert conditions. The mixture is stored in glove box.

2.2.4. Characterizations

UV-Vis absorption graphs of InP NCs are characterized by Shimadzu UV-1800 UV-VIS Spectrophotometer. XRD spectrum of InP NCs is measured by Rigaku D/MAX2500V/PC High Power XRD. Lastly, TEM images of InP NCs are taken by using JEOL JEM-2100 Normal-TEM.

2.3. Result and discussion

2.3.1. Synthesis of InP NCs at various temperature ranges

Figure 13 shows the UV-Vis absorption graphs of InP NCs synthesized at the temperature of 180, 200, 220 ℃, with fixed flow rate of 50 μl/min. 1st exciton peaks are measured at 560 nm, 600 nm and 610nm, respectively.

According to the figure, 1st exciton peak is getting red-shifted as the reaction temperature increases. This trend of results corresponds to that of the batch synthesis. With the similar behaviors of the product about red-shift of 1st exciton peak and increase of temperature, we can assume that the reaction conducted in microfluidic reactor follows the similar way of batch process.

In same flow rates, 1st exciton peak is getting broader as the temperature increases. Relative reactivity of DEAP, which is lower than that of $(TMS)_3P$, may one of the reason of broadening of the peak. As temperature increases, reaction rate is also increases. From that conditions and the difference of the reactivity of the chemicals, the products based on DEAP has more broader size distribution as reaction occurred in slower rate.

Also, reaction is processed under laminar flow. From the characteristics of the laminar flow, induced RTD (Residence Time Distribution) from current flow is affected the final size distribution of the products.

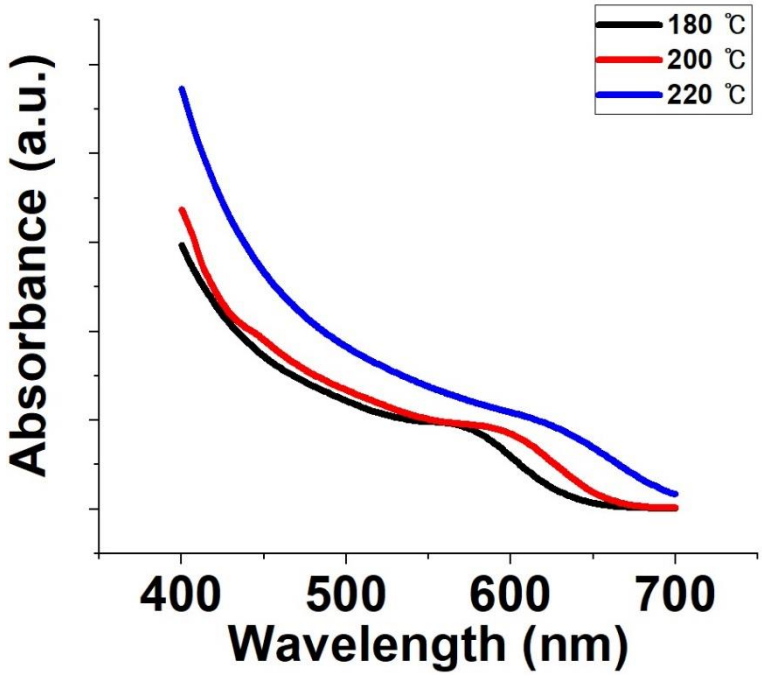

Figure 13. Absorption graph of InP NCs synthesized at 180, 200, 220 ℃ with fixed flow rate of 50 μl/min

2.3.2. Synthesis of InP NCs at various flow rates

Figure 14 shows the UV-Vis absorption graphs of InP NCs synthesized at the flow rate of 25 μl, 75 μl and 100 μl/min, with fixed temperature of 180 ℃. 1st exciton peaks are measured at ranges of 550 nm to 620nm.

From those results, it is clear the position of 1st exciton peak is affected by temperature and flow rate. As flow rate increases in the same temperature, 1st exciton peak is getting shifted to shorter wavelength range, since increase of flow rate means decrease of residence time and reaction time.

In same temperature, 1st exciton peaks of the products are broadened as the flow rate increases. It can be explained by velocity gradients in the laminar flow, which increases as flow rate increases. Velocity gradients in the flow induces the velocity differences between each velocity layers, which leads to inhomogeneous residence time and broader size distribution of the nanoparticle in the reaction flow. This trend is more notable when the temperature is getting increased.

According to the results, change of temperature to control the position of 1st exciton peak is more effective than change of flow rate in the synthesis of InP NCs through the microfluidic reactor system. The reason is, as both temperature and flow rate increases, the position and shape of the peak is more depending on the change of temperature.

In short, band-gap of InP NCs synthesized through the reactor system can be easily controlled via change of temperature and flow rate of the system. These results are corresponded to previous results from batch reactors, which the peak is shifted as temperature and reaction time is changed. In same way, the characteristics of products synthesized from microfluidic reactors are affected by the temperature and flow rate of the reactor system, which flow rate is corresponded to reaction time. The advantage of microfluidic reactor over the batch reactor is synthesis of InP NCs with various absorption peak with only modifying the temperature and flow rate, while maintaining continuous process.

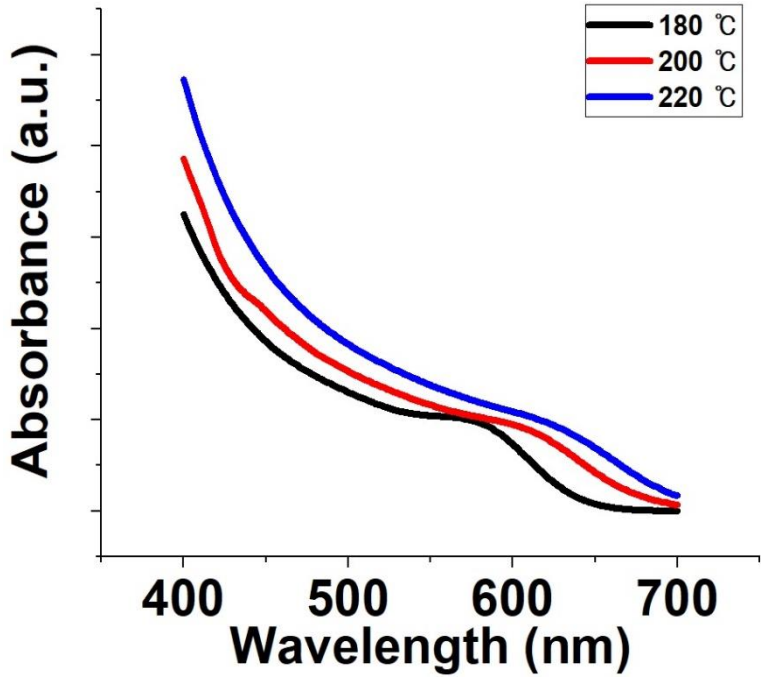

25 μl/min

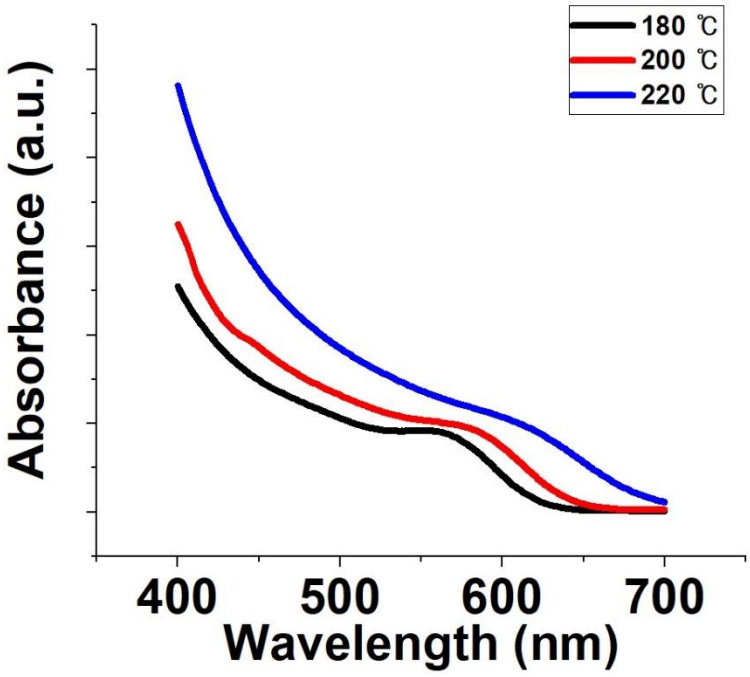

75 μl/min

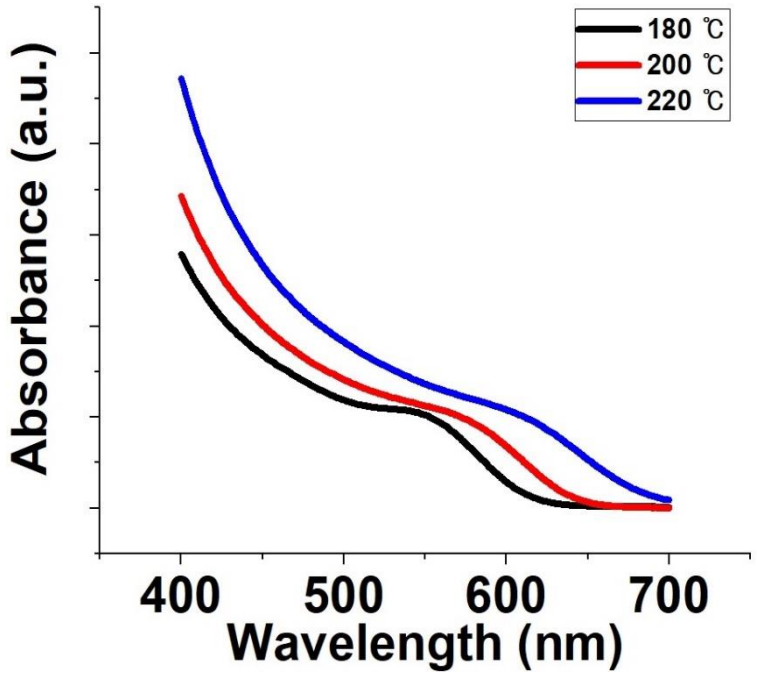

100 μl/min

Figure 14. Absorption graph of InP NCs synthesized at 25, 75 100 μl/min with fixed temperature of 180 ℃

2.3.3. Synthesis of InP NCs with halide exchange of indium precursor

Figure 15 shows the UV-Vis absorption graphs of InP NCs synthesized by changing the halide of indium precursor. (InX_3, X = Cl, Br, I)

With those so-called 'halide exchanges' of indium precursor, 1st exciton peaks of the products are getting blue-shifted as the period of halide is increased. 1st exciton peak of InP NCs synthesized by using InI_3 is measured at 450 nm and the peak of InP NCs synthesized by using $InBr_3$ is measured at 500 nm. The results show significant shift of the peak compared to that of changing temperature and flow rate.

According to previous literature work of Tessier at el., surface reaction rates are changed when halides are adsorbed on the surface of InP NC, which resulted from interaction between InP NCs and halide or steric effect. Also, surface which can adsorb additional reactant is reduced when the halide atoms are adsorbed on the surface and this effect is more dominant as the size of halide atom is getting bigger. Therefore, the surface reaction rate is decreased and eventually interrupt the growth of InP NCs. With these reasons, halide exchange affects the final size of InP NCs, which related to 1st exciton peak. The products using $InBr_3$ and InI_3 show broader peak than that of the products synthesized from $InCl_3$.[52]

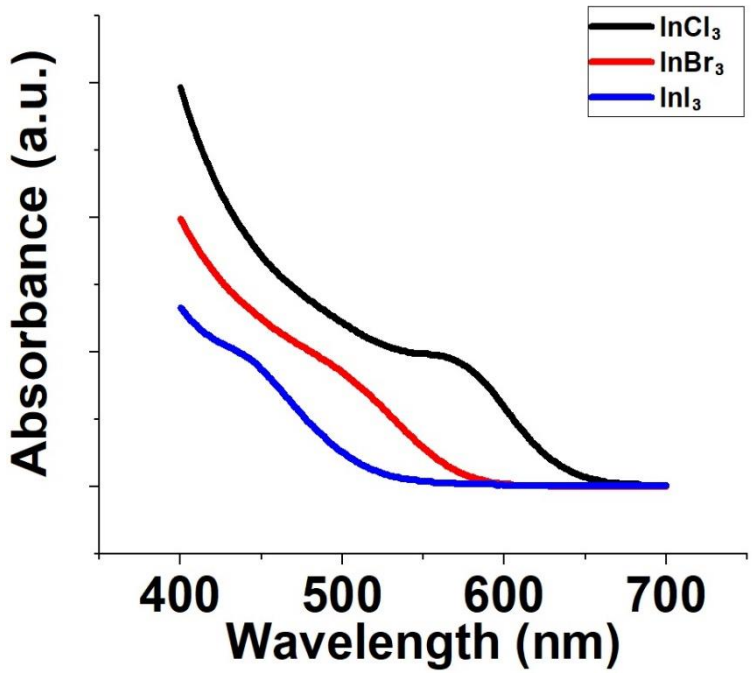

Figure 15. Absorption graph of InP NCs synthesized from different indium precursor (InX_3, X=Cl, Br, I), with fixed temperature and flow rate of 180 ℃ and 50 μl/min

2.3.4. Synthesis of InP NCs with addition of tert-dodecanethiol

Figure 16 shows the UV-Vis absorption graphs of InP NCs synthesized with addition of tert-dodecanethiol (tert-DDT), while changing the concentration of the chemical.

In InP QD synthesis, lewis base such as oleylamine competes with phosphine precursor to bond with the In-P intermediates within the reactants while composing the InP cores. This process is important to decide the size of the InP cores. DDT, as strong lewis base, also interrupt the formation of InP cores, cause to create smaller cores. From this, InP NCs with shorter absorption wavelength can be synthesized from addition of DDT.[53]

Also, the temperature and flow rate conditions of reactor system are adjusted because of the reasons mentioned previously.

As from the Figure 16, although synthesized at the conditions of higher temperature and lower flow rate than previous reference conditions, which are temperature of 180 ℃ and flow rate of 50 μl/min, 1st exciton peaks of the products are measured at much shorter wavelength, which ranges of 470 nm and 520 nm. Also, the peak of the products show more confine than previous results. We can assume that the effect of tert-DDT restricts the size of the InP NCs in certain degree, lead to decrease of size distribution. As a proof of the trend, 1st exciton peaks are getting broader as concentration of tert-DDT reduces, while the peak is moved to longer wavelength ranges.

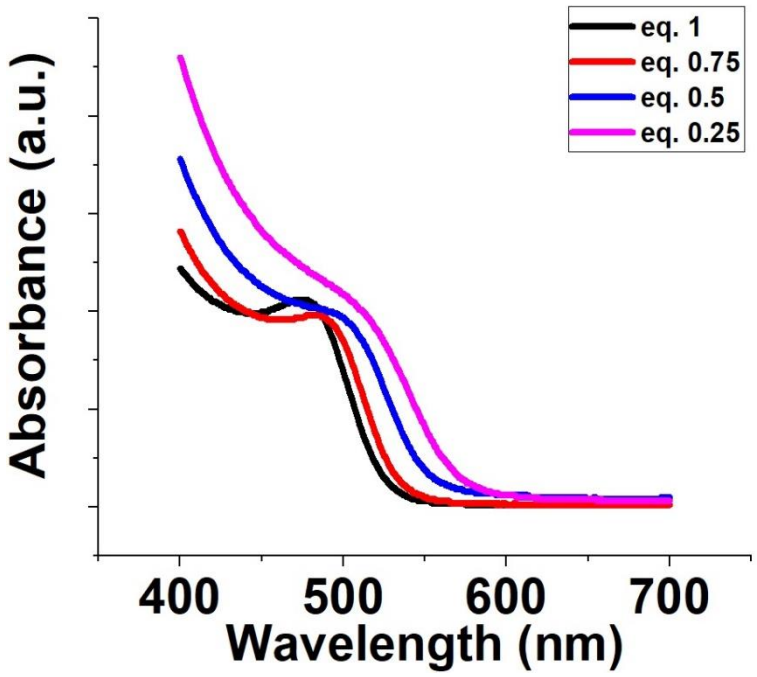

Figure 16. Absorption graph of InP NCs synthesized from tert-DDT-added precursor, with fixed temperature and flow rate of 200 ℃ and 20 μl/min

2.3.5. Comparison between MFR-based InP NCs and batch-based InP NCs

Figure 17 shows absorption graphs of samples synthesized using batch and MFR systems. Each product is synthesized at temperature of 180 ℃. Flow rate for MFR systems is set to 50 μl/min.

For the batch products, absorption graph of the products shows that the 1st exciton peak is reached to certain wavelength in 10 minutes, meaning that actual reaction of NC growth is completed in that time.

Considering a volume of microfluidic reactor, residence time of reagent flow in the reactor is calculated below 3 minutes. Comparing the products from batch and microfluidic reactor systems at 3 minutes, the 1st exciton peak of MFR products is much more red-shifted than the peak of batch products, meaning that the size of NCs from MFR is bigger than the size of batch products. The result indicates that heat transfer in the MFR systems is more efficient than that in the batch system on the same temperature condition.

1st exciton peak of MFR samples is broader than the peak of batch samples, showing that the products from MFR systems have broader size distribution.

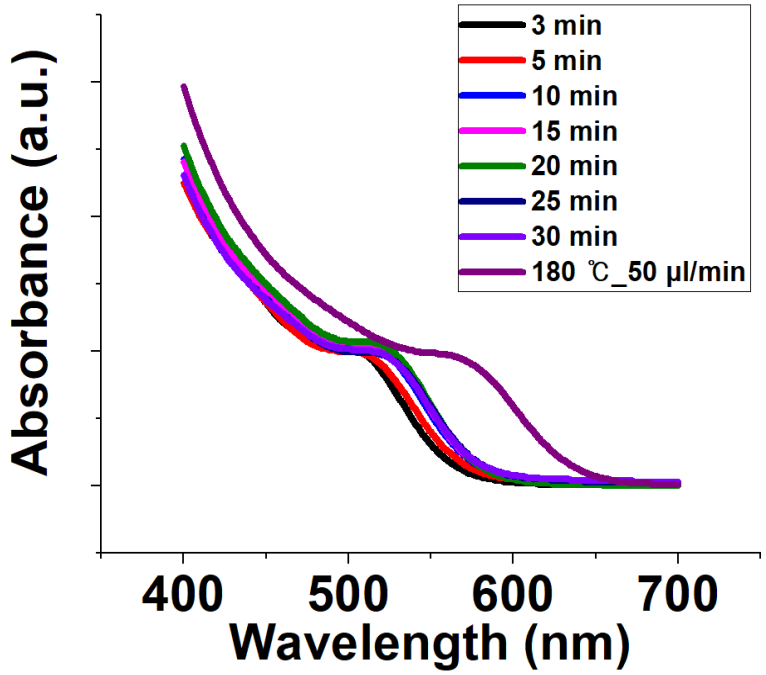

Figure 17. Absorption graphs of InP NCs synthesized from batch and microfluidic reactor

2.3.6. Characterizations

Figure 18 shows the XRD spectrum of InP NCs synthesized at the conditions of 180 ℃ and 50 μl/min. Through the spectrum, the existence of InP peak tells the products contain the component of InP. Besides InP peak, distinct peaks of ZnO are also detected. Since zinc is easy to oxidize, these peaks are mainly based on oxidized zinc, which may created during the washing step of crude solution.

From the measured peaks, the result shows the peaks corresponded to the published XRD data. Peak of (1 1 1) plate at 2Θ = 26.28, (2 2 0) plate at 2Θ = 43.58 and (3 1 1) plate at 2Θ = 51.6 are detected, meaning that the products synthesized from microfluidic reactor systems are mainly consist of zinc blende-structured InP NCs.

Figure 19 shows the TEM images of InP NCs synthesized at the same conditions. In TEM images, we can detect the crystal structure of InP NCs, meaning that the products created by using current microfluidic reactor system are same as those of the batch system. Through the 20 samples in following TEM images, the average size of synthesized NCs is calculated about 2.7 nm.

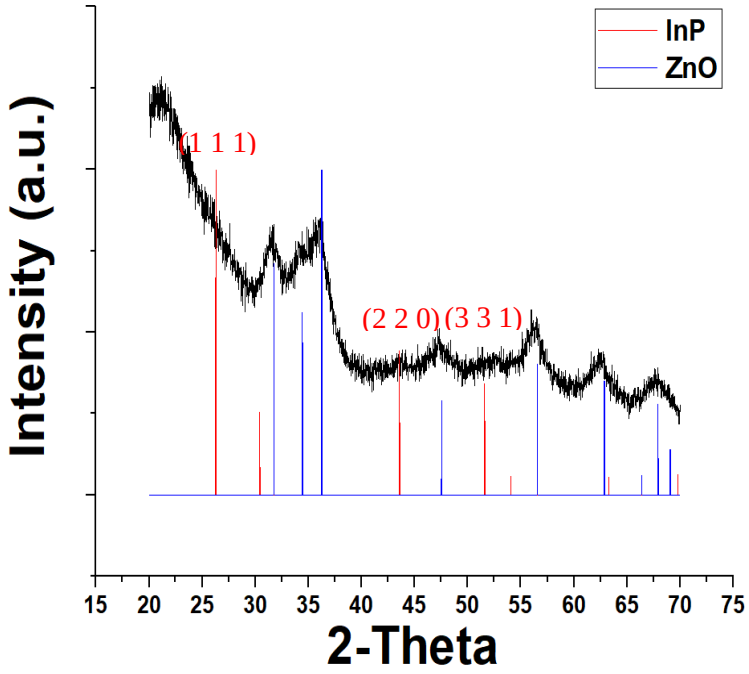

Figure 18. XRD spectrum of InP NCs synthesized at 180 ℃ and 50 μl/min

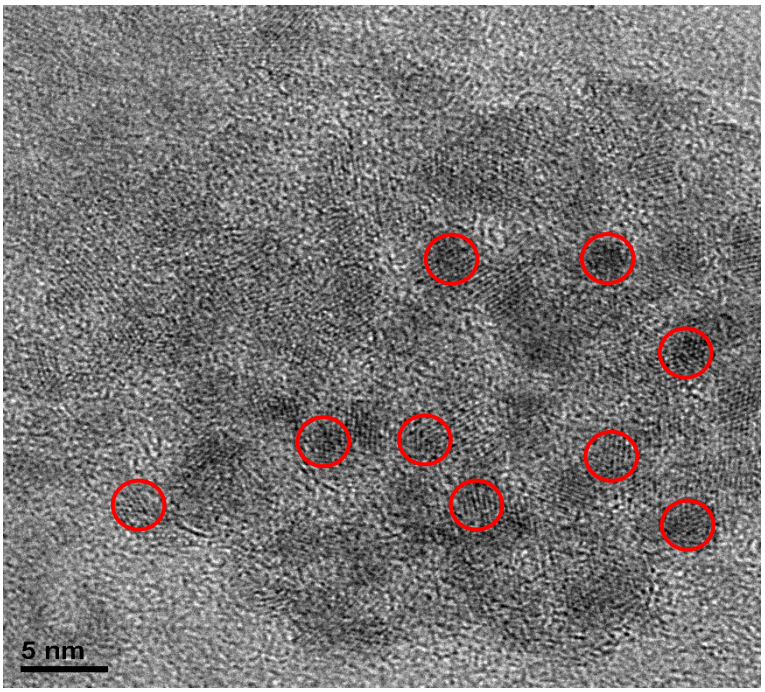

500k

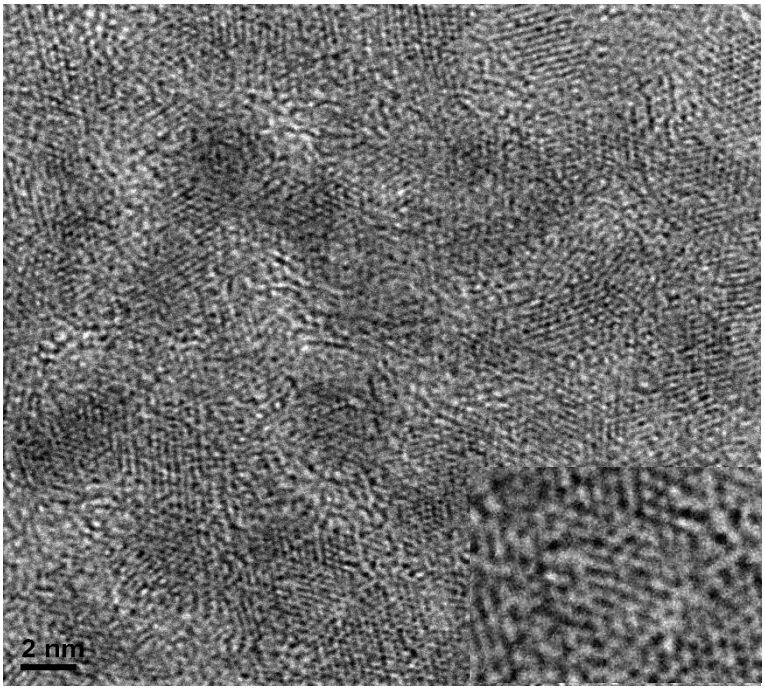

800k

Figure 19. TEM images of InP NCs synthesized at 180 ℃ and 50 μl/min

2.4. Conclusions

In this chapter, synthesis of InP NCs using aminophosphine as phosphine precursor and versatile steel reactor is shown.

For conditions of reactor system, 1st exciton peaks of InP NCs are shifted through changing the reaction temperature, flow rate, halide part of indium precursor and adding tert-DDT. Also, the behaviors of the synthesis in the microfluidic reactor system is similar from that of the batch reactor system.

As flow rate decreases, 1st exciton peaks of the products are red-shifted as residence time is increased, as well as reaction time is increased. For halide exchange of indium precursor, 1st exciton peaks are blue-shifted as the period of halide increases, which leads to the increase of the size of synthesized NCs. tert-DDT, as strong lewis base, also affects the decrease of the size of InP NCs, cause the blue-shift of 1st exciton peaks.

TEM and XRD data show crystal structures of InP NCs and detect the InP peak within the products, proving the products synthesized from microfluidic reactor system are InP NCs.

Chapter III : Synthesis of InP@ZnS Core@Shell-structured quantum dots via microfluidic reactor

3.1. Introduction

For InP NCs, they have low photoluminescence quantum yield (PLQY) as value of ~1% with only core structure. This result comes from the surface defect and lattice mismatch of InP NCs, as well as from non-radiative surface recombination sites and activation barriers for carrier detrapping.[69-72]

To resolve these issues, typically, chemicals like zinc and selenium or zinc and sulfur are used in shell growth on InP cores, to create the core@shell structure of NCs. Those shells on the surface of NCs reduce the surface defect and lattice mismatch, while increase the stability of the cores.

Core@shell-structured InP QDs can have high PLQY of 40% - 70% and narrow FWHM of 45 nm. Also, those QDs show similar ranges of emission and absorption wavelength compared to cadmium-based QDs, which are red to green.[73]

In shell growth, band-edge energy offset between core and materials used at shell growth and lattice mismatch between surfaces are important, which determine the optical properties of final products.[74] These shells also help the surface passivation of the cores.

In this chapter, synthesis of core@shell-structured InP@ZnS QDs using tert-DDT and microfluidic reactor system is described. Comparison of the products from the microfluidic reactor system with other products from conventional batch system is also conducted.

3.2. Experimental session

3.2.1. Overall setup of microfluidic reactor system

Figure 20 shows the schematics of the reactor and its system for core@shell-structure QDs. The shape of the channels is sinusoidal and each reactor parts are attached physically with bolts.

Reagents for core and shell synthesis are injected into the system with Harvard Apparatus PHD 2000 HVP Programmable Syringe Pump 70-2023 and 20 ml Harvard Apparatus steel syringes. Syringes and reactor parts are connected by 1/16" SUS316 tubes. For core synthesis part, volume of the reactor is about 160 μl. Volume of the reactor for shell growth is about 270 μl. Channel length and height of both reactor channels are 1 mm. The dimension of each reactor plates is 100 X 55 X 12 mm, as size of upper and lower plates are same. To prevent the leakage result from physical attachment of the plates with bolts, gasket made of multilayers of Teflon tapes is added. Temperature control of reactor system is conducted by feedback controller, which probe is added between the each of reactor plates with the gasket.

After the reaction is concluded, ODE is used to clean the both reactors for recycling.

The shape of channels is sinusoidal, which is same as the reactor for NC synthesis. Reasons of designing the channel shape in the reactors are similar with that of designing the NC synthesis part.

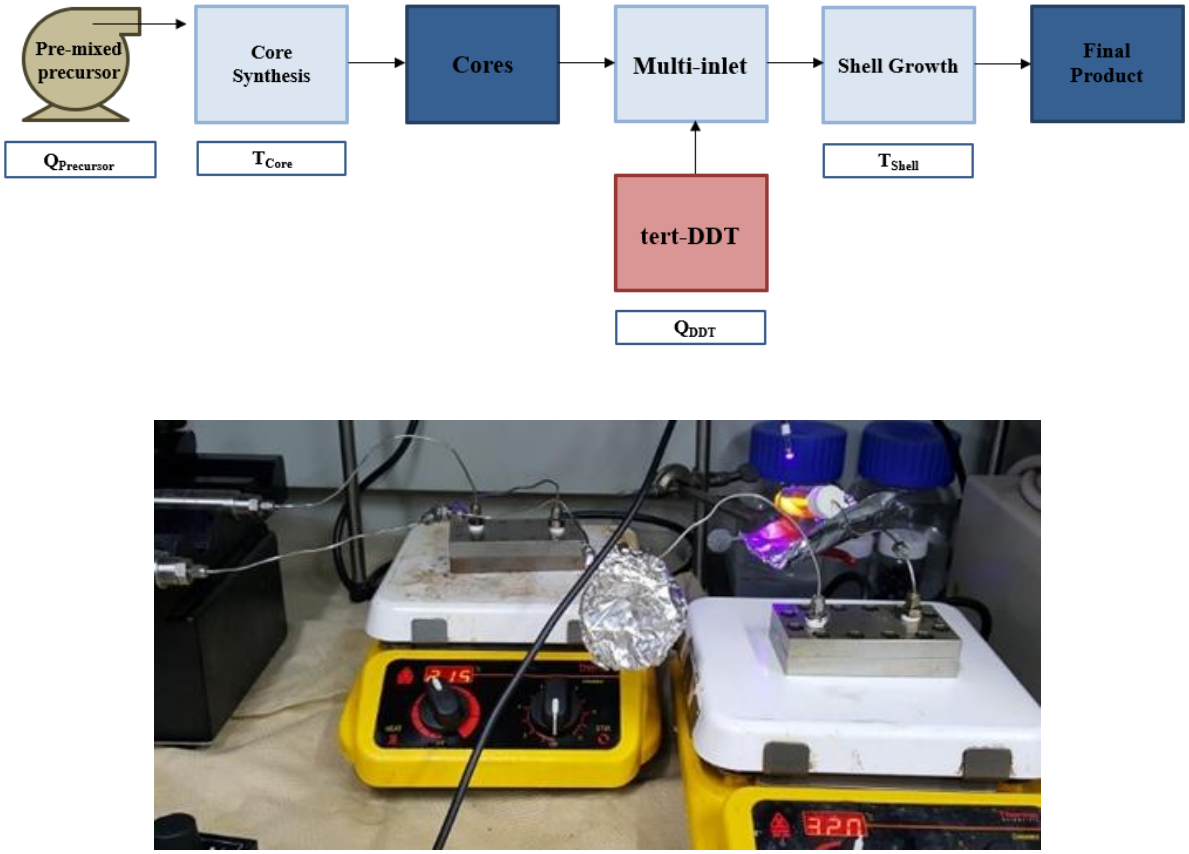

Figure 20. Schematics and image of InP@ZnS QD synthesis microfluidic reactor system

3.2.2. Chemicals

Indium(III) chloride ($InCl_3$), Zinc chloride ($ZnCl_2$), Oleylamine (97%) (OAm), tris(diethylamino)phosphine (DEAP), tert-dodecanethiol and 1-Octadecene (ODE) are purchased from Sigma-Aldrich. All the chemicals are used without further purification.

3.2.3. Stock solution for core synthesis

The process is same as mentioned in chapter II. $InCl_3$ 0.6 g, $ZnCl_2$ 1.8 g and 30 ml of oleylamine are prepared in 100 ml 2-neck round bottom flask under inert conditions. For degassing, prepared solution is heated to 120 ℃ for 90 minutes. After temperature of the mixture dropped down to RT, 2.76 ml of DEAP is injected under inert conditions. The mixture is stored in glove box.

3.2.4. Characterizations

UV-Vis absorption graphs of InP NCs are characterized by Shimadzu UV-1800 UV-VIS Spectrophotometer. PLQY is measured by Otsuka QE-2000 Quantum Efficiency Measurement System. XRD spectra of InP NCs are measured by Rigaku D/MAX2500V/PC High Power XRD. Lastly, TEM images of InP NCs are taken by using JEOL JEM-2100 Normal-TEM.

3.3. Result and discussion

3.3.1. Synthesis of InP@ZnS Core@Shell QDs and comparison between MFR samples and batch samples

Reaction process is presented in the Figure 20. For core synthesis, temperature and flow rate are set to 180 ℃ and 60 μl/min, respectively. For shell synthesis, temperature and flow rate are set to 280 ℃ and 30 μl/min, respectively. Each condition is based on the conditions of the batch process.

Figure 21 shows absorption graphs and PL spectra of core@shell-structured InP@ZnS QDs from microfluidic reactor system and conventional batch system. Figure 22 shows emissions of the products corresponded to each synthesis methods, using UV lamps.

According to the PL spectra, PLQY of InP@ZnS QDs synthesized from microfluidic reactor is about 31%, whereas PLQY of QDs from batch system is 38%. The results show that the PLQY of QDs from microfluidic reactor is similar with the data from batch system.

FWHM of QDs from microfluidic reactor is measured as 85 nm, whereas FWHM of QDs from batch system is measured as 51 nm. Measured FWHM values of each products tell that the products synthesized from microfluidic reactor system have broader size distribution than that of products from batch system. In other word, the products from batch system are more homogeneous than the products from microfluidic reactor. The main difference of size distribution between those products is based on laminar flow on the microfluidic reactor. As previously described, in nanoparticle synthesis on the microreactor, characteristics of laminar flow could induce the size distribution between each nanoparticle during the reaction.

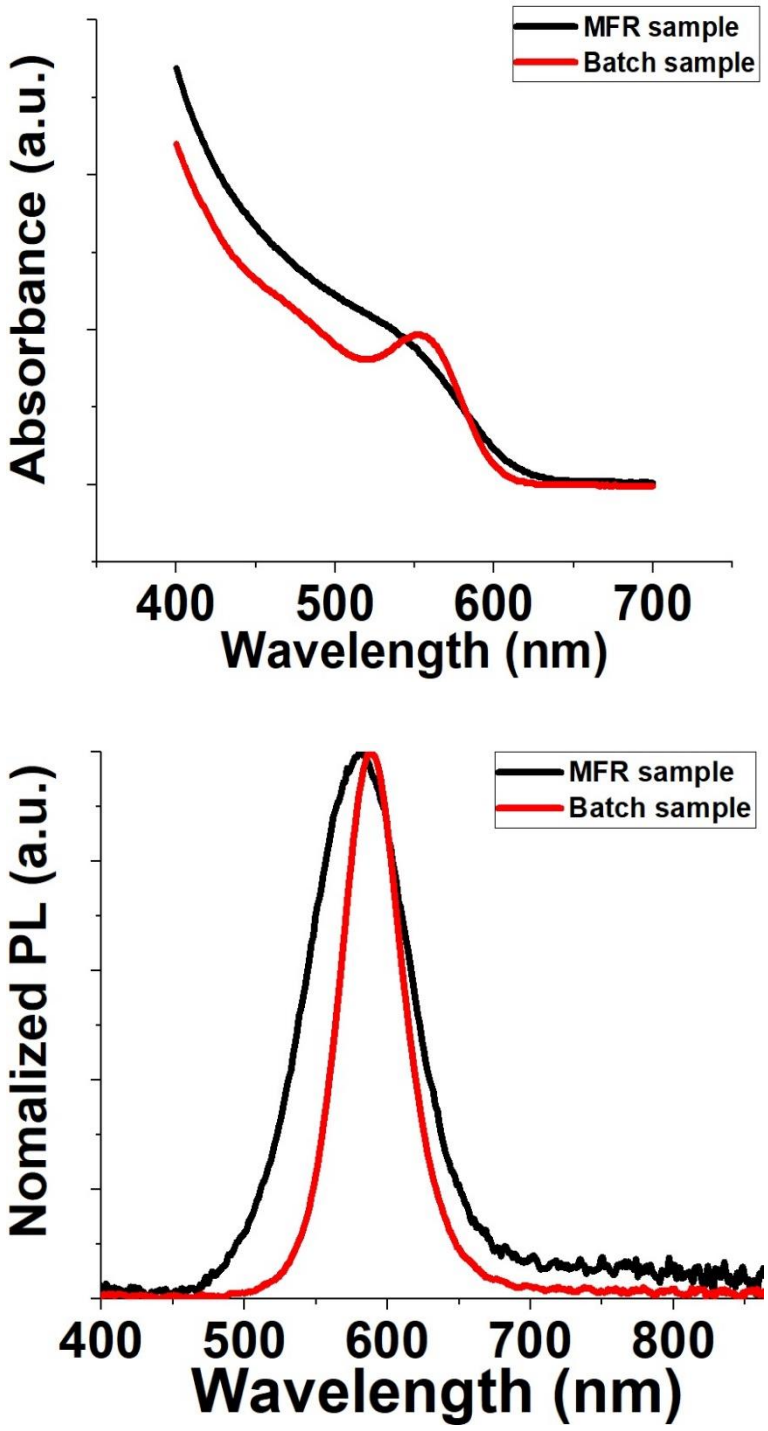

Figure 21. Absorption and PL spectra of InP@ZnS Core@Shell QDs from microfluidic reactor and conventional batch reactor

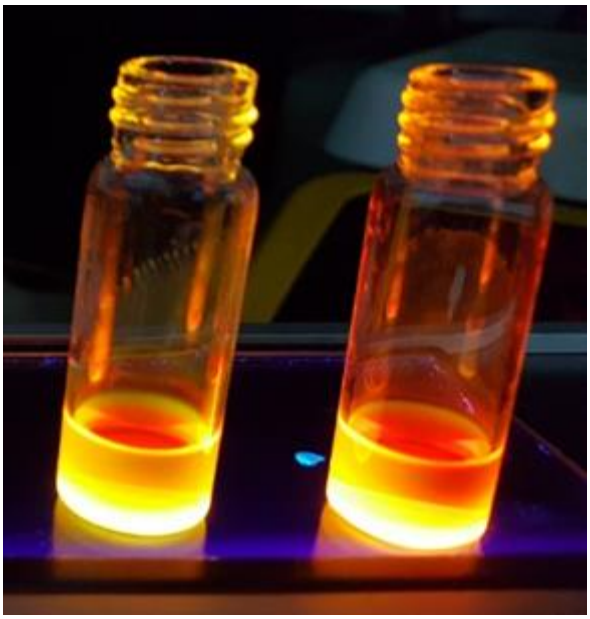

Figure 22. UV emission of the products from microfluidic reactor and conventional batch reactor (Left : MFR-based products, Right : Batch-based products)

3.3.2. Characterizations

Figure 23 shows the XRD spectrum of InP@ZnS core@shell QDs synthesized at the conditions described at 3.3.1. Through the spectrum, the existence of InP and ZnS peak tells the products contain the component of InP@ZnS QDs. Besides those peaks, distinct peaks of ZnO are also detected. Similar with XRD spectrum of InP NCs, these peaks are mainly based on oxidized zinc, which assume to be created during the washing step of crude solution.

From the measured peaks, the result shows the peaks corresponded to the published XRD data. Peak of (1 1 1) plate at $2\Theta = 26.28$, (2 2 0) plate at $2\Theta = 43.58$ and (3 1 1) plate at $2\Theta = 51.6$ are detected. This result shows that the InP cores synthesized from following systems are same NCs synthesized from previous NC synthesis. Also, following XRD data show the corresponded ZnS peaks and their plates, meaning the synthesized products from the systems are zinc blende structured-InP@ZnS QDs.

Figure 24 shows the TEM images of InP@ZnS QDs synthesized at the same conditions. In TEM images, we can detect the crystal structure of InP@ZnS QDs, proving that the products from microfluidic reactor system are same as those of the batch system. Through the 20 samples in following TEM images, the average size of synthesized QDs is calculated about 3 nm.

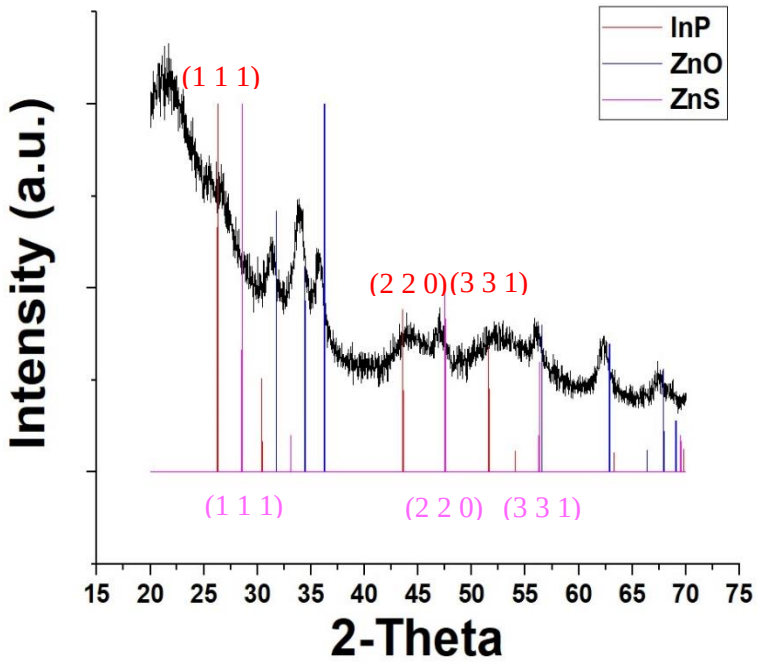

Figure 23. XRD spectrum of InP@ZnS Core@Shell QDs

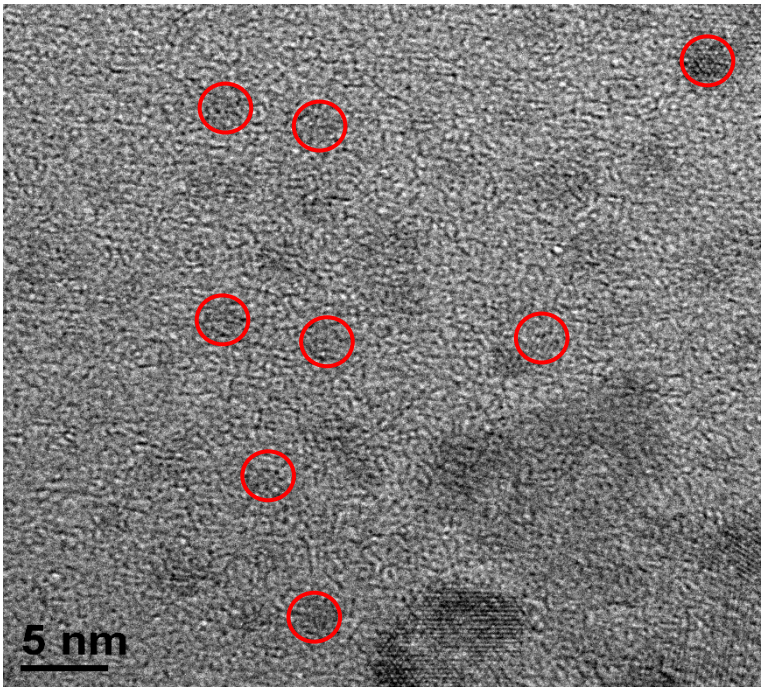

500k

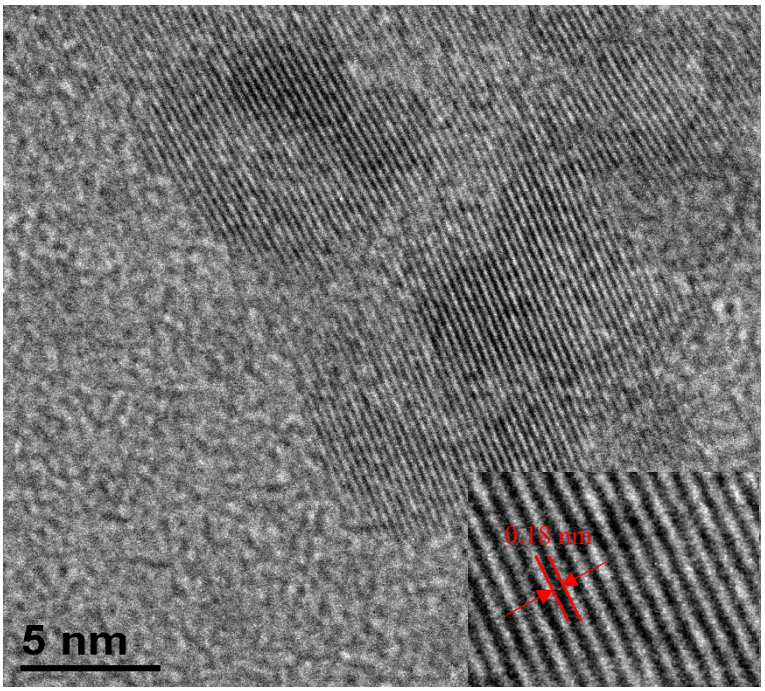

800k

Figure 24. TEM images of InP@ZnS Core@Shell QDs

3.4. Conclusions

In this chapter, synthesis of InP@ZnS core@shell-structured QDs using versatile steel reactor and aminophosphine and tert-DDT as phosphine precursor for InP Cores and shell growth material is shown.

InP@ZnS core@shell-structured QDs from microfluidic reactor have the values of PLQY and FWHM as 31%, 85 nm, respectively, whereas the QDs from batch system have the values of 38%, 51 nm, respectively. Broader size distribution of microfluidic reactor-based QDs is caused by laminar flow on the reactor.

Through TEM and XRD measurements, corresponding data prove that the products synthesized from microfluidic reactor system is similar with the products from batch system. Also, detection of InP and ZnS peaks in XRD spectra shows that the products are mainly consist of InP@ZnS QDs.

Conclusions

This thesis studied about the synthesis of aminophosphine-based InP NCs and InP@ZnS core@shell-structure QDs using versatile steel reactor system.

For synthesis of InP NCs using the reactor system, the effects of temperature and flow rate on the reaction and trend of products are studied. 1st exciton peaks of InP NCs are red-shifted as temperature increases, or flow rates decreases. In opposite conditions, 1st exciton peaks of InP NCs are blue-shifted. Band-gap control through changing halide part of indium precursor and adding tert-DDT is also studied.

These results show the possibility that microfluidic reactor can synthesize InP NCs with wide range of absorption and emission range through changing simple factors like flow rate in continuous way. Synthesized products are characterized by XRD and TEM, proving the products are same as that of batch system.

For synthesis of InP@ZnS core@shell-structured QDs, the results show the possibility of simple process based on microfluidic reactors, integrating the entire processes of core synthesis and shell growth in one system.

InP@ZnS QDs from microfluidic reactor show similar PLQY, which is 31%, with the products from batch system, which is about 38%, whereas FWHM of the products from microfluidic reactor is wider than that of the products from batch system. We assume that this problem could be solve through changing the flow patterns, such as applying segmented flow or droplet flow.

In conclusions, integrated systems based on microfluidic reactors for InP NCs and QDs give possibility of applying complex synthesis methods like SIRAL to the reactor systems, conducting the methods more convenient and fast with assuring high-quality products.

References

1. S.C.Terry; J.H.Jerman; J.B.Angell A Gas Chromatographic Air Analyzer Fabricated on a Silicon Wafer. *IEEE Trans.Electron Devices*, **1979,** *ED-26,12*, 1880-1886

2. Kirby, B.J. Micro- and Nanoscale Fluid Mechanics: Transport in Microfluidic Devices. *Cambridge University Press.*, **2010**

3. Bruus, H. Theoretical Microfluidics. *Oxford University Press.*, **2007**

4. Tabeling, P. Introduction to Microfluidics. *Oxford University Press.*, **2005**

5. Tice, Joshua D.; Song, Helen; Lyon, Adam D.; Ismagilov, Rustem F. Formation of Droplets and Mixing in Multiphase Microfluidics at Low Values of the Reynolds and the Capillary Numbers. *Langmuir*, **2003,** *19(22)*, 9127-9133.

6. Günther, Axel; Jhunjhunwala, Manish; Thalmann, Martina; Schmidt, Martin A.; Jensen, Klavs F. Micromixing of Miscible Liquids in Segmented Gas−Liquid Flow. *Langmuir*, **2005**, *21(4)*, 1547-1555.

7. K. Geyer; T. Gustafsson; P. H. Seeberger Developing continuous-flow microreactors as tools for synthetic chemists. *Synlett*, **2009**.

8. Lee, Chung-Cheng; Sui, Guodong; Elizarov, Arkadij; Shu, Chengyi Jenny; Shin, Young-Shik; Dooley, Alek N.; Huang, Jiang; Daridon, Antoine; Wyatt, Paul; Stout, David; Kolb, Hartmuth C.; Witte, Owen N.; Satyamurthy, Nagichettiar; Heath, James R.; Phelps, Michael E.; Quake, Stephen R.; Tseng, Hsian-Rong Multistep synthesis of a radiolabeled imaging probe using integrated microfluidics. *Science,* **2005**, *310(5755),* 1793-1796.

9. Baek, J.; Allen, P. M.; Bawendi, M. G.; Jensen, K. F. Investigation of indium phosphide nanocrystal synthesis using a high-temperature and high-pressure continuous flow microreactor. *Angew Chem Int Ed Engl*, **2011**, *50(3)*, 627-630.

10. Valencia, Pedro M.; Farokhzad, Omid C.; Karnik, Rohit; Langer, Robert Microfluidic technologies for accelerating the clinical translation of nanoparticles. *Nature Nanotechnology*, **2012**, *7***,** 623.

11. Wyss, H. M.; Blair, D. L.; Morris, J. F.; Stone, H. A.; Weitz, D. A. Mechanism for clogging of microchannels. *Phys Rev E Stat Nonlin Soft Matter Phys*, **2006**, *74(6 Pt 1)*, 061402.

12. Nightingale, Adrian M.; Bannock, James H.; Krishnadasan, Siva H.; O'Mahony, Flannan T. F;

Haque, Saif A.; Sloan, Jeremy; Drury, Chris; McIntyre, Robert; deMello, John C. Large-scale synthesis of nanocrystals in a multichannel droplet reactor. *Journal of Materials Chemistry A*, **2013**, *1(12)*, 4067-4076.

13. Yinuo Cheng; Xiongying Ye; Zengshuai Ma; Shuai Xie; Wenhui Wang; Toner M.; Irimia D. High-throughput and clogging-free microfluidic filtration platform for on-chip cell separation from undiluted whole blood. *Biomicrofluidics*, **2016**, *10(1)*, 014118.
14. Yang, Chun-Guang; Xu, Zhang-Run; Lee, Abraham P.; Wang, Jian-Hua A microfluidic concentration-gradient droplet array generator for the production of multi-color nanoparticles. *Lab on a Chip*, **2013**, *13(14)*, 2815-2820.
15. Brock DC A measure of success. *Chem Herit Mag*, **2011**, *29(1)*
16. Kitson, Philip J.; Rosnes, Mali H.; Sans, Victor; Dragone, Vincenza; Cronin, Leroy Configurable 3D-Printed millifluidic and microfluidic 'lab on a chip' reactionware devices. *Lab on a Chip*, **2012**, *12(18)*, 3267-3271.
17. ELVEFLOW, "Microfluidics and microfluidic devices : a review**",** https://www.elveflow.com/microfluidic-tutorials/microfluidic-reviews-and-tutorials/microfluidics-and-microfluidic-device-a-review/
18. Harrison DJ; Flury K; Seiler K; Fan Z; Effenhauser CS; Manz A Micromachining a miniaturized capillary electrophoresis based chemical analysis system on a chip. *Science*, **1993**, *261*, 895–897
19. (2001). "Microreactors - New Technology for Modern Chemistry Wolfgang Ehrfeld Volker Hessel Holger Löwe Wiley-VCH: Weinheim. 2000. 288 pp. ISBN3-527-29590-9." Organic Process Research & Development **5**(1): 89-89.
20. Jahnisch, K.; Hessel, V.; Lowe, H.; Baerns, M. Chemistry in microstructured reactors. *Angew Chem Int Ed Engl*, **2004**, *43(4)*, 406-446.
21. R. Knitter; D. Gohring; P. Risthaus; J. Hausselt Microfabrication of ceramic microreactors. *Microsystem Technologies*, **2001**, *7*, 85–90.
22. Kikutani, Y.; Hibara, A.; Uchiyama, K.; Hisamoto, H.; Tokeshi, M.; Kitamori, T. Pile-up glass microreactor. *Lab Chip*, **2002**, *2(4)*, 193-196.
23. K. F. Jensen Materials for micro- and nanofluidics. *MRS Bull.*, **2006**, *31*, 101–107.
24. Y. Xia; G. M. Whitesides Soft Lithography. *Annual Review of Materials Science*, **1998**, *28*, 153-184.
25. Grover, W. H.; von Muhlen, M. G.; Manalis, S. R. Teflon films for chemically-inert microfluidic valves and pumps. *Lab Chip*, **2008**, *8(6)*, 913-918.

26. Toke R. Henriksen; Jakob L. Olsen; Peter Vesborg; Ib Chorkendorff; Ole Hansen Highly sensitive silicon microreactor for catalyst testing. *Review of Scientific Instruments*, **2009**, *80(12)*, 124101.

27. S. Takeuchi; P. Garstecki; D.B. Weibel; G.M. Whitesides; An axisymmetric flow-focusing microfluidic device. *Adv Mater*, **2005**, *17*, 1067-1071.

28. Yang, Hongwei; Luan, Weiling; Wan, Zhen; Tu, Shan-tung; Yuan, Wei-Kang; Wang, Zhiming M. Continuous Synthesis of Full-Color Emitting Core/Shell Quantum Dots via Microreaction. *Crystal Growth & Design*, **2009**, *9(11)*, 4807-4813.

29. Tian, Zhen-Hao; Xu, Jian-Hong; Wang, Yu-Jun; Luo, Guang-Sheng Microfluidic synthesis of monodispersed CdSe quantum dots nanocrystals by using mixed fatty amines as ligands. *Chemical Engineering Journal*, **2016**, *285*, 20-26.

30. Kwon, Byoung-Hwa; Kim, Hyunki; Kim, Youngsun; Kang, Dongseok; Young Jeon, Duk Synthesis of ZnSe Quantum Dots Using a Continuous-Flow Microreactor and Their White Emission through Energy Transfer. *ECS Solid State Letters*, **2013**, *2(8)*, R27-R30.

31. Yen, Brian K. H.; Günther, Axel; Schmidt, Martin A.; Jensen, Klavs F.; Bawendi, Moungi G. A Microfabricated Gas–Liquid Segmented Flow Reactor for High-Temperature Synthesis: The Case of CdSe Quantum Dots. *Angewandte Chemie*, **2005**, *117(34)*, 5583-5587.

32. Marre, Samuel; Park, Jongnam; Rempel, Jane; Guan, Juan; Bawendi, Moungi G.; Jensen, Klavs F. Supercritical Continuous-Microflow Synthesis of Narrow Size Distribution Quantum Dots. *Advanced Materials*, **2008**, *20(24)*, 4830-4834.

33. Chan, Emory M.; Alivisatos, A. Paul; Mathies, Richard A. High-Temperature Microfluidic Synthesis of CdSe Nanocrystals in Nanoliter Droplets. *Journal of the American Chemical Society*, **2005**, *127(40)*, 13854-13861.

34. Nightingale, A. M.; J. C. de Mello Controlled Synthesis of III–V Quantum Dots in Microfluidic Reactors. *ChemPhysChem*, **2009**, *10(15)*, 2612-2614.

35. Kyungnam, Kim; Sohee, Jeong; Ju Yeon, Woo; Chang-Soo, Han Successive and large-scale synthesis of InP/ZnS quantum dots in a hybrid reactor and their application to white LEDs. *Nanotechnology*, **2012**, *23(6)*, 065602.

36. Lignos, Ioannis; Stavrakis, Stavros; Nedelcu, Georgian; Protesescu, Loredana; deMello, Andrew J.; Kovalenko, Maksym V. Synthesis of Cesium Lead Halide Perovskite Nanocrystals in a Droplet-Based Microfluidic Platform: Fast Parametric Space Mapping. *Nano Letters*, **2016**, *16(3)*, 1869-1877.

37. Buzaglo, Matat; Shtein, Michael; Regev, Oren Graphene Quantum Dots Produced by Microfluidization. *Chemistry of Materials*, **2016**, *28(1)*, 21-24.

38. Lignos, Ioannis; Protesescu, Loredana; Stavrakis, Stavros; Piveteau, Laura; Speirs, Mark J.; Loi, Maria A.; Kovalenko, Maksym V.; deMello, Andrew J. Facile Droplet-based Microfluidic Synthesis of Monodisperse IV–VI Semiconductor Nanocrystals with Coupled In-Line NIR Fluorescence Detection. *Chemistry of Materials*, **2014**, *26(9)*, 2975-2982.

39. Lim, Hosub; Woo, Ju Young; Lee, Doh C.; Lee, Jinkee; Jeong, Sohee; Kim, Duckjong Continuous Purification of Colloidal Quantum Dots in Large-Scale Using Porous Electrodes in Flow Channel. *Scientific Reports*, **2017**, *7*, 43581.

40. Shen, Yi; Weeranoppanant, Nopphon; Xie, Lisi; Chen, Yue; Lusardi, Marcella R.; Imbrogno, Joseph; Bawendi, Moungi G.; Jensen, Klavs F. Multistage extraction platform for highly efficient and fully continuous purification of nanoparticles. *Nanoscale*, **2017**, *9(23)*, 7703-7707.

41. Anikeeva, Polina O.; Halpert, Jonathan E.; Bawendi, Moungi G.; Bulović, V. Quantum Dot Light-Emitting Devices with Electroluminescence Tunable over the Entire Visible Spectrum. *Nano Letters*, **2009**, *9(7)*, 2532-2536.

42. Caruge, J. M.; Halpert, J. E.; Wood, V.; Bulovic, V.; Bawendi, M. G. Colloidal quantum-dot light-emitting diodes with metal-oxide charge transport layers. *Nat Photon*, **2008**, *2(4)*, 247-250.

43. Sun, Liangfeng; Choi, Joshua J.; Stachnik, David; Bartnik, Adam C.; Hyun, Byung-Ryool; Malliaras, George G.; Hanrath, Tobias; Wise, Frank W. Bright infrared quantum-dot light-emitting diodes through inter-dot spacing control. *Nat Nano*, **2012**, *7(6)*, 369-373.

44. Chan, Warren C. W.; Nie, Shuming Quantum Dot Bioconjugates for Ultrasensitive Nonisotopic Detection. *Science*, **1998**, *281(5385)*, 2016-2018.

45. Wang, Dayang; Rogach, Andrey L.; Caruso, Frank Semiconductor Quantum Dot-Labeled Microsphere Bioconjugates Prepared by Stepwise Self-Assembly. *Nano Letters*, **2002**, *2(8)*, 857-861

46. Jaiswal, Jyoti K.; Mattoussi, Hedi; Mauro, J. Matthew; Simon, Sanford M. Long-term multiple color imaging of live cells using quantum dot bioconjugates. *Nature Biotechnology*, **2003**, *21(1)*, 47-51.

47. Plass, Robert; Pelet, Serge; Krueger, Jessica; Grätzel, Michael; Bach, Udo Quantum Dot Sensitization of Organic−Inorganic Hybrid Solar Cells. *The Journal of Physical Chemistry B*, **2002**, *106(31)*, 7578-7580.

48. Bang, Jin Ho; Kamat, Prashant V. Quantum Dot Sensitized Solar Cells. A Tale of Two Semiconductor Nanocrystals: CdSe and CdTe. *ACS Nano*, **2009**, *3(6)*, 1467-1476.

49. Danek, Michal; Jensen, Klavs F.; Murray, Chris B.; Bawendi, Moungi G. Synthesis of Luminescent Thin-Film CdSe/ZnSe Quantum Dot Composites Using CdSe Quantum Dots Passivated with an Overlayer of ZnSe. *Chemistry of Materials*, **1996**, *8(1)*, 173-180.

50. Dabbousi, B. O.; Rodriguez-Viejo, J.; Mikulec, F. V.; Heine, J. R.; Mattoussi, H.; Ober, R.; Jensen, K. F.; Bawendi, M. G. (CdSe)ZnS Core−Shell Quantum Dots: Synthesis and Characterization of a Size Series of Highly Luminescent Nanocrystallites. *The Journal of Physical Chemistry B*, **1997**, *101(46)*, 9463-9475.

51. Protesescu, Loredana; Yakunin, Sergii; Bodnarchuk, Maryna I.; Krieg, Franziska; Caputo, Riccarda; Hendon, Christopher H.; Yang, Ruo Xi; Walsh, Aron; Kovalenko, Maksym V. Nanocrystals of Cesium Lead Halide Perovskites (CsPbX3, X = Cl, Br, and I): Novel Optoelectronic Materials Showing Bright Emission with Wide Color Gamut. *Nano Letters*, **2015**, *15(6)*, 3692-3696.

52. Tessier, Mickael D.; Dupont, Dorian; De Nolf, Kim; De Roo, Jonathan; Hens, Zeger Economic and Size-Tunable Synthesis of InP/ZnE (E = S, Se) Colloidal Quantum Dots. *Chemistry of Materials*, **2015**, *27(13)*, 4893-4898.

53. Park, Joong Pill; Lee, Jae-Joon; Kim, Sang-Wook Highly luminescent InP/GaP/ZnS QDs emitting in the entire color range via a heating up process. *Scientific Reports*, **2016**, *6*, 30094

54. Stein, Jennifer L.; Mader, Elizabeth A.; Cossairt, Brandi M. *The Journal of Physical Chemistry Letters*, **2016**, *7(7)*, 1315-1320.

55. Hailegnaw, Bekele; Kirmayer, Saar; Edri, Eran; Hodes, Gary; Cahen, David Rain on Methylammonium Lead Iodide Based Perovskites: Possible Environmental Effects of Perovskite Solar Cells. *The Journal of Physical Chemistry Letters*, **2015**, *6(9)*, 1543-1547.

56. Akkerman, Quinten A.; D'Innocenzo, Valerio; Accornero, Sara; Scarpellini, Alice; Petrozza, Annamaria; Prato, Mirko; Manna, Liberato Tuning the Optical Properties of Cesium Lead Halide Perovskite Nanocrystals by Anion Exchange Reactions. *Journal of the American Chemical Society*, **2015**, *137(32)*, 10276-10281.

57. Kulbak, Michael; Cahen, David; Hodes, Gary How Important Is the Organic Part of Lead Halide Perovskite Photovoltaic Cells? Efficient CsPbBr3 Cells. *The Journal of Physical Chemistry Letters*, **2015**, *6(13)*, 2452-2456.

58. Leo, Karl Perovskite photovoltaics: Signs of stability. *Nat Nano*, **2015**, *10(7)*, 574-575.

59. Micic, Olga I.; Curtis, Calvin J.; Jones, Kim M.; Sprague, Julian R.; Nozik, Arthur J. Synthesis and Characterization of InP Quantum Dots. *The Journal of Physical Chemistry*, **1994**, *98(19)*, 4966-4969.

60. Allen, Peter M; Walker, Brian J; Bawendi, Moungi G. Mechanistic Insights into the Formation of InP Quantum Dots. *Angewandte Chemie International Edition*, **2010**, *49(4)*, 760-762.

61. Gary, Dylan C.; Terban, Maxwell W.; Billinge, Simon J. L.; Cossairt, Brandi M. Two-Step

Nucleation and Growth of InP Quantum Dots via Magic-Sized Cluster Intermediates. *Chemistry of Materials*, **2015**, *27(4)*, 1432-1441.

62. Song, Woo-Seuk; Lee, Hye-Seung; Lee, Ju Chul; Jang, Dong Seon; Choi, Yoonyoung; Choi, Moongoo; Yang, Heesun Amine-derived synthetic approach to color-tunable InP/ZnS quantum dots with high fluorescent qualities. *Journal of Nanoparticle Research*, **2013**, *15(6)*, 1750.
63. Xie, Renguo; Battaglia, David; Peng, Xiaogang Colloidal InP Nanocrystals as Efficient Emitters Covering Blue to Near-Infrared. *Journal of the American Chemical Society*, **2007**, *129(50)*, 15432-15433.
64. Li, Liang; Reiss, Peter One-pot Synthesis of Highly Luminescent InP/ZnS Nanocrystals without Precursor Injection. *Journal of the American Chemical Society*, **2008**, *130(35)*, 11588-11589.
65. Li, Liang; Protière, Myriam; Reiss, Peter Economic Synthesis of High Quality InP Nanocrystals Using Calcium Phosphide as the Phosphorus Precursor. *Chemistry of Materials*, **2008**, *20(8)*, 2621-2623.
66. Tessier, Mickael D.; De Nolf, Kim; Dupont, Dorian; Sinnaeve, Davy; De Roo, Jonathan; Hens, Zeger Aminophosphines: A Double Role in the Synthesis of Colloidal Indium Phosphide Quantum Dots. *Journal of the American Chemical Society* **2016**, *138(18)*, 5923-5929.
67. Buffard, Aude; Dreyfuss, Sébastien; Nadal, Brice; Heuclin, Hadrien; Xu, Xiangzhen; Patriarche, Gilles; Mézailles, Nicolas; Dubertret, Benoit Mechanistic Insight and Optimization of InP Nanocrystals Synthesized with Aminophosphines. *Chemistry of Materials*, **2016**, *28(16)*, 5925-5934.
68. Christian, Ippen; Benjamin, Schneider; Christopher, Pries; Stefan, Kröpke; Tonino, Greco; Andreas, Holländer Large-scale synthesis of high quality InP quantum dots in a continuous flow-reactor under supercritical conditions. *Nanotechnology*, **2015**, *26(8)*, 085604.
69. Olga I. Mićić; Julian Sprague; Zhenghao Lu; Arthur J. Nozik Highly efficient band-edge emission from InP quantum dots. *Applied Physics Letters,* **1996**, *68(22),* 3150-3152.
70. Adam, S.; Talapin, D. V.; Borchert, H.; Lobo, A.; McGinley, C.; de Castro, A. R.; Haase, M.; Weller, H.; Moller, T. The effect of nanocrystal surface structure on the luminescence properties: photoemission study of HF-etched InP nanocrystals. *J Chem Phys*, **2005**, *123(8)*, 084706.
71. Mićić, Olga I.; Nozik, Arthur J.; Lifshitz, Efrat; Rajh, Tijana; Poluektov, Oleg G.; Thurnauer, Marion C. Electron and Hole Adducts Formed in Illuminated InP Colloidal Quantum Dots Studied by Electron Paramagnetic Resonance. *The Journal of Physical Chemistry B*, **2002**, *106(17)*, 4390-4395.
72. S.-H. Kim; R. H. Wolters; J. R. Heath Photophysics of size-selected InP nanocrystals: Exciton recombination kinetics. *The Journal of Chemical Physics*, **1996**, *105(18)*, 7957-7963.

73. Ramasamy, Parthiban; Kim, Nayeon; Kang, Yeon-Su; Ramirez, Omar; Lee, Jong-Soo Tunable, Bright, and Narrow-Band Luminescence from Colloidal Indium Phosphide Quantum Dots. *Chemistry of Materials*, **2017**, *29(16)*, 6893-6899.

74. Bajwa, Pooja; Gao, Feng; Nguyen, Anh; Omogo, Benard; Heyes, Colin D. Role of the Inner Shell Architecture on Quantum Yield and Blinking Dynamics in Core/Multi-Shell Quantum Dots. *Chemphyschem : a European journal of chemical physics and physical chemistry*, **2016**, *17(5)*, 731-740.